Published in final edited form as:
Nat Cell Biol. 2020 February ; 22(2): 235–245. doi:10.1038/s41556-020-0462-7.

Small RNA-mediated transgenerational silencing of histone genes impairs fertility in piRNA mutants

Giorgia Barucci[#1,2], **Eric Cornes**[#1], **Meetali Singh**[#1], **Blaise Li**[3], **Martino Ugolini**[1,4], **Aleksei Samolygo**[1,5], **Celine Didier**[1], **Florent Dingli**[6], **Damarys Loew**[6], **Piergiuseppe Quarato**[1,2], **Germano Cecere**[1,†]

[1]Mechanisms of Epigenetic Inheritance, Department of Developmental and Stem Cell Biology, Institut Pasteur, UMR3738, CNRS, Paris, 75015 France

[2]Sorbonne Université, Collège doctoral, F-75005 Paris, France

[3]Bioinformatics and Biostatistics Hub – C3BI, Institut Pasteur, USR 3756, CNRS, Paris, 75015 France

[4]Scuola Normale Superiore, Pisa, Italy

[5]Moscow Institute of Physics and Technology, Moscow, Russia

[6]Institut Curie, PSL Research University, Centre de Recherche, Laboratoire de Spectrométrie de Masse Protéomique, Paris, France

[#] These authors contributed equally to this work.

Abstract

PIWI-interacting RNAs (piRNAs) promote fertility in many animals. Yet, whether this is due to their conserved role in repressing repetitive elements (REs) remains unclear. Here, we show that the progressive loss of fertility in *Caenorhabditis elegans* lacking piRNAs is not caused by derepression of REs or other piRNA targets, but rather mediated by the epigenetic silencing of all the replicative histone genes. In the absence of piRNAs, downstream components of the piRNA

[†]Corresponding author. germano.cecere@pasteur.fr.

Data availability

All the sequencing data (GRO-seq, RNA-seq, and small RNA-seq from total lysate or immunoprecipitation experiments) are available at the Gene Expression Omnibus (GEO) under accession code GSE125601. The mass spectrometry proteomics data have been deposited to the ProteomeXchange Consortium via the PRIDE partner repository with the dataset identifier PXD012557. All other data supporting the findings of this study are available from the corresponding author on reasonable request.

Author Contributions

G.C. identified and developed the core questions addressed in the project and analyzed the results of all experiments. G.B. performed most of the experiments and helped in the analysis of the results. E.C. Conceived and generated all the CRISPR-Cas9 lines used in this study, designed and performed the experiment using catalytic mutant of CSR-1, and performed all the confocal live imaging experiments. M.S. performed all the Co-immunoprecipitation and immunoprecipitation experiments for mass spectrometry and Co-IPs. F.D. and D.L. performed the mass spectrometry and analyzed the data together with M.S. and G.C. B.L. performed the bioinformatic analysis of all the sequencing data. M.U. performed some RNA extraction and the RT-qPCR experiment. A.S. performed the brood size of the RNAi experiments under the supervision of G.B. C.D. performed the brood size of some RNAi and crossing experiments together with G.C. P.Q. performed the GRO-seq. E.C. and P.Q. contributed to collect some RNA samples used for the initial RNA-seq experiments. G.C. wrote the paper with the contribution of G.B., E.C., M.S., B.L.

Competing Interests: All the authors declare no competing interests.

Europe PMC Funders Author Manuscripts

pathway relocalize from germ granules and piRNA targets to histone mRNAs to synthesize antisense small RNAs (sRNAs) and induce transgenerational silencing. Removal of the downstream components of the piRNA pathway restores histone mRNA expression and fertility in piRNA mutants, and the inheritance of histone sRNAs in wild-type worms adversely affects their fertility for multiple generations. We conclude that the sRNA-mediated silencing of histone genes impairs fertility of piRNA mutants and may serve to maintain piRNAs across evolution.

Introduction

Among different classes of endogenous small RNAs in animals, PIWI-interacting RNAs (piRNAs) play a conserved role in repressing transposons and other repetitive elements (REs)[1], and in several animal species the loss of piRNAs causes sterility[2]. Because of the role of piRNAs in transposon silencing, the sterility phenotype observed in animal lacking piRNAs is commonly believed to be caused by derepression of REs and consequently DNA damage[3]. However, non-transposon derived piRNAs promote fertility in mouse[4], and a piRNA-independent function of one of the PIWI proteins, MIWI, has been implicated in male fertility[5]. Therefore, the requirement of piRNAs and PIWI for animal fertility can be uncoupled from their role in transposon silencing and might be due to additional piRNA regulatory functions. In *C. elegans*, mutations in components of the piRNA pathway show progressive loss of fertility across generations, which ultimately leads to a sterile population of worms[6]. This transgenerational phenotype is often temperature dependent and reversible whereby animals gradually become sterile at elevated temperature and recover their fertility when grown at lower temperature[7–10]. Thus, whether the role of piRNAs in promoting fertility depends on the silencing of REs or other epigenetic mechanisms remains a matter of debate[11].

The majority of *C. elegans* piRNAs are independently transcribed in the germline from thousands of genomic loci and do not have sequence complementarity to REs[12–16]. However, they regulate their targets even by imperfect complementarity[17,18]. Thus, any REs or other germline-expressed RNA sequences, including protein-coding transcripts are potential targets and their regulation can also contribute to promote fertility. *C. elegans* piRNAs do not directly silence the expression of their targets, but trigger the accumulation of small single-stranded antisense 22G-RNAs, which are loaded into Worm-specific Argonaute proteins (WAGOs). These constitute the downstream effector factors of the piRNA-induced silencing pathway and silence the complementary targets at the transcriptional and the post-transcriptional levels[8,19,20]. PIWI and its downstream effectors localize to specific perinuclear compartment called germ granules, and some of the structural components of germ granules also participate in heritable RNAi[21–23].

Here, we investigate the mechanisms underlying the transgenerational loss of fertility in population of *C. elegans* lacking piRNAs. We show that the removal of piRNAs is not sufficient to derepress protein-coding and RE transcripts targeted by the piRNA pathway. Instead, we found that in the absence of piRNAs, the downstream effectors of piRNA-induced silencing complex relocalize from piRNA targets to histone mRNAs. This process

Europe PMC Funders Author Manuscripts

leads to the accumulation of 22G-RNAs antisense to all the replicative histone genes and to the transgenerational silencing of histone mRNAs, which ultimately lead to sterile animals.

Results

piRNA targets are not desilenced in *piwi* mutant

To understand the reduced fertility and transgenerational sterility observed in piRNA mutants[6,12,14], we identified transcripts directly regulated by piRNAs. We combined small RNA sequencing (sRNA-seq) with strand-specific RNA sequencing (RNA-seq) and compared mutants of the *C. elegans* PIWI protein PRG-1 with wild-type worms, using populations of synchronized young adult worms of the null allele *prg-1(n4357)*[14] almost sterile at 20°C (Extended Data Fig. 1a). To identify piRNA-dependent 22G-RNA protein-coding targets, we selected 1017 protein-coding genes from which substantially reduced levels of 22G-RNAs were produced (< 4-fold) in the *prg-1(n4357)* mutant compared to wild-type worms. Only 6% (67 genes) of these mRNA transcripts became up-regulated (> 2-fold; padj <0.05) (Fig. 1a). Analysis of 958 RE families revealed that 154 REs had reduced 22G-RNAs (< 2-fold) in *prg-1(n4357)* compared to wild-type worms, yet only three RE families were significantly up-regulated (> 2-fold; padj < 0.05) (Fig. 1b). We also used uniquely mapped reads to analyze the expression of approximately 60,000 discrete REs[24], and found that less than 100 individual REs were significantly up-regulated (≥ 2-fold and padj < 0.05) in *piwi* mutant compared to wild-type worms (Extended Data Fig. 1b, d). Therefore, the decrease in 22G-RNAs antisense to protein-coding genes or REs was not sufficient to derepress them, and they were likely kept repressed by nuclear RNAi and/or chromatin factors[24–26]. Indeed, RNA-seq analysis and RT-qPCR of individual REs in the mutant of the nuclear Argonaute HRDE-1, a downstream effector of the piRNA pathway that acts at the transcriptional level, resulted in a larger number of up-regulated REs compared to *prg-1(n4357)* mutant (Extended Data Fig. 1b, d). Nonetheless, the *hrde-1 (tm1200)* mutant analyzed was not sterile and showed only a mild reduced fertility compared to wild-type worms (Extended Data Fig. 1a), suggesting that the derepression of REs might not be correlated with the piRNA mutant phenotype. These results also suggest that piRNAs might only be required to initiate, and not to maintain, the silencing of their targets as proposed by previous research[19,27–29].

Histone mRNA silencing correlates with transgenerational sterility in *piwi* mutant

The RNA-seq and sRNA-seq analyses also revealed several protein-coding genes that showed reduced mRNA levels and increased 22G-RNAs in *prg-1(n4357)* compared to wild-type worms (Fig. 1a), suggesting they had been silenced by small RNAs. The majority of these transcripts corresponded to the replicative histone mRNAs (Fig. 1a), and most of the histone gene clusters acquired a substantial number of 22G-RNAs causing their complementary mRNAs to become substantially down-regulated (Fig. 1c). We also analyzed by RT-qPCR mRNA levels in the mutant of the piRNA biogenesis factor PRDE-1[30], and observed a substantial depletion of histone mRNAs (Extended Data Fig. 1c). Mutants of the nuclear Argonaute HRDE-1 did not silence histone mRNAs (Extended Data Fig. 1c, e) and nascent RNA sequencing (nRNA-seq) revealed only a mild down-regulation of some histone genes in *prg-1(n4357)* compared to wild-type (Extended Data Fig. 1f, g), indicating that the

down-regulation of the histone genes occurred at the post-transcriptional level in piRNA mutants.

In *C. elegans*, histone mRNA silencing using RNA interference (RNAi) is sufficient to cause sterility[31,32]. We, therefore, tested whether histone mRNA silencing correlated with piRNA mutant transgenerational loss of fertility. We generated a CRISPR-Cas9 null allele of the PIWI protein PRG-1, selected two independently-edited CRISPR-Cas9 lines and propagated isogenic populations of homozygote *piwi* mutant and wild-type worms (Fig. 1f). We maintained these lines for 10 generations until the *piwi* mutant became almost completely sterile (Fig. 1d), sampling the populations using RNA-seq and sRNA-seq. Mutant worms propagated for two generations after homozygosis (F4) showed no phenotypic differences compared to wild-type worms (Fig. 1d) and RNA-seq analysis showed very few gene expression changes (Extended Data Fig. 2a). At later generations, individuals from the *piwi* mutant isogenic population started to display fertility defects, including full sterility in some individuals, until the population became almost completely sterile after 10 generations (Fig. 1d). These results correlated with substantial gene expression changes across generations (Extended Data Fig. 2a-c). The progressive loss of fertility was accompanied by a gradual reduction of histone mRNA transcripts and a gain of 22G-RNAs antisense to histone mRNAs (Fig. 1e and Extended Data Fig. 2d). The modest desilencing of piRNA-dependent 22G-RNA protein-coding and RE targets did not correlate with the progressive loss of fertility (Extended Data Fig. 2d-f). To evaluate the impact of histone mRNA silencing on histone protein levels in germ cells, we generated a CRISPR-Cas9 null allele of PIWI in a transgenic strain expressing a single-copy of histone H2B::mCherry in the germline. Live imaging of wild-type worms confirmed that the H2B::mCherry was normally expressed in the germline and incorporated into chromosomes (Fig. 1g, Extended Data Fig. 2h). However, *piwi* mutants showed significantly reduced levels of H2B::mCherry in germline nuclei of animals with reduced fertility (Fig. 1g, h and Extended Data Fig. 2g). Western blotting analysis confirmed the reduced levels of H2B::mCherry in populations of *piwi* mutant worms (Fig. 1i), and Chromatin Immunoprecipitation (ChIP) experiments revealed reduced incorporation of H2B::mCherry into the chromatin of *piwi* mutant animals (Fig. 1j). These results are in accordance with the observed defect in chromosome compaction in pachytene nuclei of sterile *piwi* mutant animals (Extended Data Fig. 2h), which can be a consequence of the lack of histone incorporation into chromatin. Altogether, these results suggest that the transgenerational silencing of histone mRNAs, and not the desilencing of piRNA targets, correlates with the progressive loss of fertility observed in *piwi* mutants.

The downstream component of the PIWI pathway, WAGO-1, targets histone mRNAs for silencing

To identify RNAi factors involved in histone mRNA silencing we asked whether Argonaute proteins downstream of PIWI in the piRNA-induced silencing pathway might ectopically load small RNAs derived from histone mRNA transcripts. We identified several Argonaute proteins interacting with PIWI by mass spectrometry, among which many are known to participate in piRNA-induced silencing[20] (Fig. 2a and Supplementary Table 1a). The most highly enriched PIWI-interacting Argonaute protein was WAGO-1, which plays a role in the post-transcriptional silencing of piRNA targets[19,33]. We generated a FLAG tagged version of

WAGO-1 and confirmed the interaction between WAGO-1 and PIWI by mass spectrometry and Co-immunoprecipitation (Co-IP) experiments (Fig. 2c, and Extended Data Fig. 4a). Next, we immunoprecipitated WAGO-1 associated 22G-RNAs in wild-type and *piwi* mutant backgrounds. In the wild-type background WAGO-1 was loaded with 22G-RNAs derived from piRNA-dependent protein-coding targets (Fig. 2d), and was not enriched in 22G-RNAs from histone mRNAs (Fig. 2d). In the *piwi* mutant WAGO-1 was instead enriched in histone 22G-RNAs, and the loading of 22G-RNAs derived from piRNA-dependent 22G-RNA targets was significantly decreased (Fig. 2d). Furthermore, in *piwi* mutant worms, WAGO-1 decreases its interaction with mRNAs from piRNA-dependent 22G-RNA targets and instead binds to histone mRNAs (Extended Data Fig. 3a). These results indicate that WAGO-1 relocalized from piRNA-dependent targets to histone mRNAs in a 22G-RNA-dependent manner, suggesting that WAGO-1 is one of the Argonaute proteins that promotes histone mRNA silencing in piRNA mutant worms.

WAGO-1 gradually loses interaction with germ granule components upon *piwi* mutation

The quantification by mass spectrometry of PIWI-interacting proteins revealed, in addition to Argonaute proteins and 22G-RNA biogenesis factors, the enrichment of specific germ granule components, which are also known to participate in heritable RNAi[21–23] (Fig. 2a-c, and Supplementary Table 1a). WAGO-1 also interacts with some germ granule factors, and preferentially with DEPS-1 (Fig 2b, c, Extended Fig. 4a, and Supplementary Table 1b), a germ granule component known to participate in RNAi[34]. Many of these factors act downstream of the piRNAs to promote RNA silencing across generations[8,19,20,22,23]. Therefore, PIWI and piRNAs might help to initiate the formation of the piRNA-induced silencing complex in germ granules. To study whether the interactions between the downstream components of the piRNA-induced silencing complex are perturbed upon removal of PIWI proteins, we quantified WAGO-1-interacting proteins by mass spectrometry in wild-type compared to three progressive generations of *piwi* mutants. Our analysis revealed that the interactions between WAGO-1 and germ granule components gradually diminished across generations in absence of PIWI protein (Fig. 3a, b). Instead, WAGO-1 interaction with some Argonaute protein, such as PPW-1 and the WAGO-1-interacting 22G-RNA biogenesis factor RDE-12[35], was maintained even in late generation of *piwi* mutants (Fig. 3a, b). Taking together, these results suggest that the loss of interaction between WAGO-1 and germ granule components might affect WAGO-1 localization. To test this hypothesis, we performed live imaging of WAGO-1 and the germ granule component PGL-1 in wild-type and *piwi* mutant. Live imaging of a CRISPR-Cas9 strain expressing WAGO-1::GFP in wild-type worms confirmed its predominant perinuclear germ granule localization (Fig. 3c), as previously observed[33]. However, in late generations of *piwi* mutant, WAGO-1 lost its germ granule localization and remained mainly cytoplasmic (Fig. 3c). We confirmed this results by immunostaining experiments using CRISPR-Cas9 WAGO-1::FLAG strain in wild-type and *piwi* mutant worms (Extended Data Fig. 3b). Live imaging of the germ granule component PGL-1 in *piwi* mutant showed that the loss of WAGO-1 germ granule localization was not caused by a disruption of germ granule assembly (Fig. 3c), since PGL-1 granules were still formed even in sterile animals (Extended Data Fig. 3c). In addition, live imaging of the Argonaute protein CSR-1, which does not belong to the piRNA pathway, showed germ granule and cytoplasmic localization

in wild-type and *piwi* mutant worms, indicating that the loss of germ granule localization in *piwi* mutant is specific to the WAGO-1 Argonaute (Figure 3c and Extended Data Fig. 3c).

The CSR-1 pathway triggers the biogenesis of histone 22G-RNAs

The data presented so far suggest that in absence of PIWI, another RNAi pathway is responsible to trigger the biogenesis and loading of histone 22G-RNAs into WAGOs. The proteomic analysis of PIWI-interacting proteins revealed the interaction with the Argonaute CSR-1 (Fig. 2a and Supplementary Table 1a), which is known to counteract piRNA-silencing on mRNAs[36,37] and to promote histone biogenesis[38]. We confirmed this interaction by Co-IP experiments using a FLAG tagged CRISPR-Cas9 strain of CSR-1 (Extended Data Fig. 4a). We also analyzed CSR-1-interacting proteins by mass spectrometry and found, in addition to known components of the CSR-1 pathway, interactions with PIWI and WAGO-1 and many of their RNAi- and germ granule-interacting proteins (Fig. 4a, Extended Data Fig. 4d, and Supplementary Table 1c). However, some germ granule components, such as DEPS-1, appear to specifically interact only with PIWI and WAGO-1 (Fig. 4a, Extended Data Fig. 4a, b). Nonetheless, the piRNA and the CSR-1 pathways shared many interactors (Fig. 4a), including WAGO-1, and in absence of PIWI, WAGO-1 might preferentially interact with CSR-1 in the cytoplasm. To confirm this hypothesis, we performed Co-IP experiments that show interaction between WAGO-1 and CSR-1 also in *piwi* mutant (Fig. 4b and Extended Data Fig. 4e), even though these mutant animals have lost WAGO-1 germ granule localization and have reduced germline tissue and decreased levels of WAGO-1 compared to wild-type worms (Fig. 3c, and Extended Data Fig. 4c, e). CSR-1 is known to bind histone mRNAs and is thought to participate in the 3'end cleavage of histone mRNAs[38] together with its interacting stem-loop binding protein CDL-1[39] (Fig. 4a, Extended Data Fig. 4d). Metaprofile analysis of histone 22G-RNAs in *piwi* mutant showed a strong bias towards the end of the histone genes (Extended Data Fig. 4f), right upstream to the location of the stem-loop structure bound by CDL-1 (Fig. 4c). Thus, in the absence of PIWI the histone mRNA 3'-end cleavage by CSR-1 and CDL-1 may trigger the production of histone 22G-RNAs loaded into WAGO-1. To test this hypothesis, we mutated the catalytic domain of CSR-1 by CRISPR-Cas9 and crossed this strain with the *piwi* mutant. We observed a substantial reduction of histone 22G-RNAs in *piwi* mutant animals where the catalytic activity of CSR-1 was zygotically abolished (Fig. 4d). Similar results were obtained by using *csr-1* RNAi treatment in the *piwi* mutant (Extended Data Fig. 4g). Moreover, RNAi treatment of CDL-1 results in a slight reduction of 22G-RNAs in the region corresponding to the location of the stem-loop structure and spreading of 22G-RNAs along the coding region towards the 5' end (Extended Data Fig. 4h). These results suggest that the interaction between CSR-1 and CDL-1 help to focus the cleavage activity of CSR-1 in proximity of the stem loop structure, and this triggers the synthesis and loading of histone 22G-RNAs into the WAGO pathway in absence of PIWI.

Inactivation of downstream components of the piRNA pathway restores histone expression and *piwi* mutant fertility

To determine whether the histone 22G-RNAs cause the transgenerational loss of fertility in piRNA mutant worms, we set out to rescue the fertility defects by inactivating the downstream piRNA factors responsible for the production of 22G-RNAs. MUT-16 is one of

the biogenesis factors that promote the synthesis of 22G-RNAs loaded into WAGOs[40] and interacts with PIWI (Fig. 2a). RNAi depletion of MUT-16 (Fig. 5a) over two generations restored *piwi* mutant fertility (Fig. 5b), and *piwi* mutant worms treated continuously with *mut-16* RNAi did not become sterile (Extended Data Fig. 5a, b). Additionally, *mut-16* RNAi treatment on sterile *piwi* mutant worms was sufficient to restore their fertility. RNAi depletion of WAGO-1 also restored the fertility of sterile *piwi* mutant worms (Fig. 5g). However, the restored fertility was lower than *mut-16* RNAi treatment, suggesting that other Argonaute proteins might participate in histone mRNA silencing in *piwi* mutant (Fig. 5g). Indeed, RNAi treatment of *ppw-1* or *ppw-2*, the two other Argonautes that interact with CSR-1, PIWI and WAGO-1 (Fig. 4a), showed rescued *piwi* mutant fertility (Extended Data Fig. 5 c, d). Instead, RNAi knock down of HRDE-1 did not recover *piwi* fertility, likely because histone mRNAs are mainly silenced at the post-transcriptional level (Extended Data Fig. 5c, d). To demonstrate that the recovered fertility in *mut-16* RNAi treated animals was specifically promoted by the desilencing of histone mRNAs we analyzed 22G-RNAs and mRNAs using RNA-seq. The reduction of histone 22G-RNAs correlated with increased expression of the replicative histone mRNAs in *mut-16* RNAi treated animals (Fig 5c, d). Five piRNA-dependent targets showed a modest re-silencing signature, suggesting that they were unlikely to contribute to the recovered fertility (Extended Data Fig. 5e). Absence of re-silencing of REs was observed upon *mut-16* RNAi treatment in the *piwi* mutant background (Fig. 5e). The rescued fertility of piRNA mutants treated with *mut-16* RNAi was instead accompanied by further desilencing of REs (Fig. 5e and Extended Data Fig. 5f). In addition, WAGO-1 remained cytoplasmic in those fertile animals, suggesting no restoration of canonical WAGO-1 silencing complex in germ granules (Fig. 5f). Moreover, WAGO-1 and CSR-1 interaction persisted even in absence of histone 22G-RNAs (Extended Data Fig. 4e), indicating that this interaction is upstream of histone 22G-RNA synthesis. Collectively, these results suggest that the removal of histone 22G-RNAs upon *mut-16* RNAi treatment and not the re-silencing of REs restored the fertility of *piwi* mutants.

Inheritance of *piwi* mutant phenotype and histone 22G-RNAs in wild-type worms

To test whether inheritance of histone 22G-RNAs is sufficient to transmit a *piwi*-like phenotype in wild-type worms, we outcrossed *prg-1(n4357)* hermaphrodites with wild-type males (Fig. 6a). We used worms from later generations of the *piwi* mutants, which were almost completely sterile, to select individuals expressing high levels of histone 22G-RNAs (Fig. 6b). In 2 out of 5 crosses we selected three heterozygotes (+/-) F1 lines in each cross, and propagated two F2 homozygote (-/-) *prg-1(n4357)* mutant and one wild-type (+/+) animals from each line and analyzed the brood of the F3 progeny (Fig. 6b and Extended Data Fig. 6a-d). The homozygote *prg-1(n4357)* mutants remained almost completely sterile after the cross (Fig. 6b, and Extended Data Fig. 6a, c). The homozygote wild-type (+/+) animals displayed a *piwi*-like phenotype, showing reduced fertility compared to the parental P0 wild-type (Fig. 6b, and Extended Data Fig. 6a, c). To determine whether this reduced fertility was caused by inherited DNA mutations, we performed brood size assay on all the progeny from one of the most affected F3 worms. All the resulting F4 animals showed increased fertility compared to the parental F3 animal (Fig. 6c), indicating that DNA mutation was not responsible for the observed phenotype in outcrossed wild-type worms. To further exclude possible genetic effects of the parental *prg-1(n4357)* mutant allele, we

repeated the outcross experiment (Fig. 6a) using one of the *piwi* mutant allele generated by CRISPR-Cas9, and observed the same results (Fig. 6d and Extended Data Fig. 6e). In addition, we propagated the selected outcrossed homozygote wild-type lines for three subsequent generations and observed a gradual recovery of fertility (Fig. 6d), even though some wild-type lines did not completely recover the parental level of fertility. Sequencing 22G-RNAs from three of the outcrossed homozygote wild-type lines after 6 generations revealed inherited histone 22G-RNAs (Fig. 6e). We also crossed heterozygote hermaphrodite animals with wild-type males, and we observed similar inherited phenotype in wild-type worms (Fig. 6f, g and Extended Data Fig. 6f). Based on these results, we propose that the maternal transmission of a pool of histone 22G-RNAs into wild-type worms can epigenetically affects their fertility.

Discussion

Here we have revealed the epigenetic mechanism underlying the transgenerational loss of fertility in *C. elegans* piRNA mutants. We have shown that the *piwi* phenotype is not related to the role of piRNAs in repressing REs, but results from the inheritance of a pool of 22G-RNAs that are antisense to histone mRNAs, leading to the post-transcriptional silencing of all the replicative histone genes. Previous reports have proposed that the sterility of *piwi* mutants is a consequence of “heritable stress” caused by REs derepression, which lead to a form of adult diapause in late generations of *piwi* mutant[6,41]. Our RNA-seq analysis of almost 60,000 individual REs has shown that only less than 100 REs are upregulated in *piwi* mutant across generations, and their upregulation does not correlate with the sterility phenotype. Instead, we have documented the transgenerational silencing of histone mRNAs by 22G-RNAs, which causes a reduction in the pool of histone proteins and lack of incorporation of histones into the chromatin. The lack of histone incorporation into chromatin and defects in chromosome compaction can explain the reported cell death and germ cell atrophy in sterile *piwi* mutant animals[41]. Thus, we propose that the inheritance of histone 22G-RNAs underlie the “heritable stress” that ultimately lead to sterile animals.

Our results show that the silencing of histone genes is caused by targeting of the WAGO pathway away from piRNA-dependent 22G-RNA targets to histone mRNAs. This process requires several worm generations, possibly because the WAGO pathway can still be recruited to piRNA-dependent 22G-RNA targets in the absence of PIWI for several generations. We speculate that the germ granule localization of WAGO-1 and its interaction with specific germ granule components, such as DEPS-1, help to maintain the piRNA-induced WAGO-1 silencing complex on piRNA targets even in absence of PIWI for certain generations. However, the interaction between WAGO-1 and DEPS-1 might not be stable without PIWI, and WAGO-1 interaction with CSR-1 might be favored in the cytoplasm allowing WAGO-1 silencing complex to localize on histone mRNAs. In support of this hypothesis, we have shown that WAGO-1 interaction with germ granule components is gradually decreased across generations of *piwi* mutant, even though it is still capable of interacting in the cytoplasm with the 22G-RNA biogenesis factor RDE-12 and the Argonaute CSR-1. In addition to WAGO-1, other downstream Argonautes of the piRNA pathway might relocalize on histone mRNAs in absence of PIWI. We have shown that two of these Argonaute, PPW-1 and PPW-2, which also interacts with CSR-1 in wild-type

worms, are required for histone mRNA silencing in *piwi* mutant, suggesting they might also relocalize on histone mRNAs similarly to WAGO-1.

Our results suggest that the cleavage of histone pre-mRNAs by CSR-1 is required to facilitates the synthesis and loading of histone 22G-RNAs by the WAGO pathway in absence of PIWI. CSR-1 may also cleave other germline mRNA targets[42]. However, we did not observe silencing of CSR-1 mRNA targets by the WAGO pathway in *prg-1* mutants. One possibility is that the amount of cleavage product from CSR-1 mRNA targets is much lower than the cleaved histone mRNAs. Alternatively, other factors, such as mRNA-specific nucleotide sequences[18,43], may prevent germline mRNAs from becoming targets of the WAGO pathway in the absence of piRNAs.

Our results, together with previous reports[28,29], suggest that piRNAs might only be required to initiate and not to maintain the silencing of REs. Nonetheless, a continuous synthesis of piRNAs is required in each generation to repress potential RE invasions. We speculate that the piRNA-driven production of WAGO-bound 22G-RNAs we observed against more than a thousand of protein-coding genes functions to maintain the piRNA-induced silencing complex in readiness to silence foreign RNAs. Nonetheless, it is unclear how the piRNA pathway can be evolutionary retained if it is only “waiting” for a potential invasion. Previous works have shown the physiological function of PIWI in regulating some germline mRNA targets[44,45]. Based on our results, we propose a model where the coupling between the lack of piRNAs and the consequent silencing of histone genes, initiated by CSR-1 and CDL-1, acts as the evolutionary force that maintains a functional piRNA-induced silencing pathway (Extended Data Fig. 7). Thus, the processing of histone mRNAs by CSR-1 and the co-evolution and co-existence of both the piRNA and the CSR-1 pathways could be an important evolutionary force in keeping the piRNA pathway in some nematode lineages. Indeed, nematode clades that have lost the piRNA pathway also lack CSR-1[46], except for clade III nematodes[47], which retain the CSR-1 pathway. We speculate that clade III nematodes escaped the sterility phenotype because they have polyadenylated histone mRNAs[48], which likely do not require CSR-1 and CDL-1 for their processing.

We have observed the transmission of a *piwi*-like phenotype in wild-type worms through small RNAs. These results implicate small RNAs as molecules capable of transmitting epigenetic information between individuals and across generations, over and above the information encoded in their genomes.

Methods

C. elegans Strains

Strains were maintained at 20°C, using standard methods[49]. Bristol N2 was the wild-type reference strain used. The complete list of strains used in this study is provided in Supplementary Table 2.

Generation of CRISPR-Cas9 lines

CRISPR-Cas9 alleles were generated by microinjecting Cas9/guideRNA ribonucleoprotein complexes in hermaphrodite gonads as described in[50].

Guide RNA in vitro transcription, repair templates and microinjection—Unique and specific guide RNA sequences were selected using the off-target prediction CRISPR Design tool at http://crispr.mit.edu/. Gene specific guide RNA sequences were included in a 60nt forward oligo containing: a 22nt T7 promoter sequence followed by the 20nt gene specific guide RNA sequence and a 18nt sequence with homology to the 5' tracrRNA scaffold sequence included in the AP0905 plasmid (kindly provided by Geraldine Seydoux lab). This forward oligo was used in combination with a reverse oligo homologous to the 3'sequence of the tracrRNA, to amplify by PCR from the AP0905 plasmid, a dsDNA template for guide RNA in vitro transcription. PCRs were performed using a High-Fidelity Phusion DNA Polymerase (Thermo Scientific) and PCR products were purified using the DNA clean and concentrator kit (Zymo Research). Guide RNAs were in vitro transcribed for 3 hours at 37°C from ~ 400ng template PCR products using T7 RNA polymerase kit (New England Biolabs) following manufacturer's instructions. In vitro transcribed RNAs were DNAse treated using 2U of Turbo DNase (Ambion) and purified using RNA clean and concentrator kit (Zymo Research). For single nucleotide modifications or small tag edits, we used single-stranded oligonucleotides containing ≈ 33bp homology arms as repair templates ordered from IDT as standard 4nM ultramer oligos. In the case of larger edits such as fluorescent protein tag sequences, we generated dsDNA repair templates by amplifying eGFP or mCherry from PJJR82 and PJJR83 plasmids (kindly provided by M. Boxem lab) by PCR using specific oligos containing ≈ 33bp homology arms. Silent mutations were included when needed in the repair templates to modify either the PAM sequence or the guide RNA seed region to prevent Cas9 from cleaving the repair template. To improve screening efficiency, a guide RNA targeting *dpy-10* was used as a Co-CRISPR marker as described in[51]. Injection mixes were prepared as described in[50].

Briefly, 10μL mixes contained typically: 10-15μM Cas9-NLS protein (Institut Pasteur core facility), 300ng/μL in vitro transcribed *dpy-10* guide RNA, 1μg/μL in vitro transcribed target gene guide RNA, 0.44 pmol/μL of *dpy-10* ssODN repair template and 0.8 pmol/μL of target gene ssODN repair template or 300ng/uL target gene dsDNA repair template.

Screening and validation of CRISPR-Cas9 alleles—Modified target loci were screened by PCR using target gene specific oligos. For the generation of the *piwi* mutant, a STOP codon (UAG) followed by a NheI restriction site was introduced after the 5th codon of PRG-1. We selected this region because it contained a PAM sequence that allowed us to target specifically *prg-1* and not *prg-2,* a gene with high sequence homology to *prg-1.* Primers specific to *prg-1* were used to amplify the genomic region spanning the edited locus and a restriction enzyme digestion was performed on the PCR amplicon. After digestion with NheI, the wild type allele produces an 889 nt band whereas edited fragments produce two bands (616 nt + 275 nt). We used the same guide RNA to introduce a 3xFLAG::2xHA epitope tag after the 6th codon of PRG-1. Similarly, we have used a *csr-1* specific guide RNA to introduce a 3xFLAG::1xHA epitope tag after the first codon of short isoform of CSR-1 to tag both the long and the short isoforms of the protein. We used the 3xFLAG::HA::CSR-1 as an entry strain to introduce mCherry to create a fluorescently tagged mCherry::3xFLAG::HA::CSR-1 strain. We also introduced a 3xFLAG::OLLAS tag right after the start codon of *wago-1.* Due to the high sequence homology between *wago-1*

and *wago-2* we couldn't find a completely specific *wago-1* guide RNA close to the start codon. We used a guide RNA targeting both *wago-1* and *wago-2* and designed gene specific primers to screen for worms where only *wago-1* was edited. To control for unwanted modifications at the *wago-2* locus we sequenced the *wago-2* targeted region and confirmed the absence of any type of edit. Similarly to the mCherry tagged version of CSR-1, we used the 3xFLAG::OLLAS::WAGO-1 as an entry strain to introduce eGFP in the 3xFLAG::OLLAS region to obtain a fluorescently tagged 3xFLAG::GFP::OLLAS::WAGO-1 strain. To generate a catalytic dead mutant of *csr-1*, we substituted a conserved aspartic acid residue by an alanine (D769A), a modification previously shown to be sufficient to abolish the catalytic activity of CSR-1 in vitro[52].

The nucleotide changes introduced to modify the codon in addition to the silent changes added to the repair removed a MaeII restriction site in our *csr-1(D769A)* edited locus. We screened the presence of our edit in PCR products based on resistance to restriction using MaeII. All the loci edited in this study were verified by sequencing locus specific PCR products. A detailed list of guide RNAs, ssDNA and dsDNA repair templates and primers used for genotyping is provided in Supplementary Table 3.

Balancers and genetics

csr-1(D769A) mutants were balanced into nT1[qIs51], a reciprocal translocation between chromosome IV and V containing a recessive lethal marker causing the embryonic lethality of homozygous balanced worms. In addition, nT1[qIs51] carries a balancer associated dominant *unc* phenotype and GFP transgenes which allow the visual identification of heterozygous animals[53].

We used a COPAS Biosorter (Union Biometrica) to set up a fluorescent-based sorting approach that allowed us to obtain large synchronized homozygous *csr-1(D769A)* populations for genome wide analysis of small RNAs.

csr-1(D769A) (IV) /nT1[qIs51] (IV;V) ; *piwi/piwi* (I) strain was obtained after a three-step crossing strategy summarized here as follows. First, wild type males were mated with a single early generation *piwi* mutant hermaphrodite. Second, the resulting F1 *piwi* / + (I) males were mated with *csr-1(D769A)* (IV) /nT1[qIs51] (IV;V) balanced worms. The non-GFP males resulting from the crossed progeny of this second cross are *csr-1(D769A)/+* (IV) and in 50 % of the cases are *piwi*/+ (I). Third, we pooled at least 5 of these non-GFP males and crossed with *csr-1(D769A)* IV /nT1[qIs51] balanced worms to introduce the piwi allele in heterozygosis in the progeny. We screened for GFP positive (/nT1[qIs51] balanced) F1 worms from this cross carrying either *csr-1 wildtype* or the *csr-1(D769A)* allele and the *piwi/+* mutation. From these two different lines we singled out GFP balanced progeny individuals to finally obtain the *csr-1(D769A)* (IV) /nT1[qIs51] (IV;V) ; *piwi/piwi* (I) and their corresponding control *+/+* /nT1[qIs51] (IV;V) ; *piwi/piwi* (I) animals.

Genotyping

For genotyping, single worms were manually picked in 20 μL of Worm Lysis Buffer (30 mM Tris pH 8, 8 mM EDTA,100 mM NaCl, 0.7% NP40, 0.7% Tween 20) containing 100 μg/mL Proteinase K. The solution was incubated at 65°C for 1 hour followed by Proteinase K

inactivation at 95°C for 15 minutes. A fraction of the lysate (5μL) was used as template for a PCR reaction using gene specific oligos. For genotyping, single worms were manually picked in 20 μL of Worm Lysis Buffer (30 mM Tris pH 8, 8 mM EDTA,100 mM NaCl, 0.7% NP40, 0.7% Tween 20) containing 100 μg/mL Proteinase K. The solution was incubated at 65°C for 1 hour followed by Proteinase K inactivation at 95°C for 15 minutes. A fraction of the lysate (5μL) was used as template for a PCR reaction using gene specific oligos. The sequences of primers used for genotyping is provided in Supplementary Table 3.

piwi crossing/mating experiments

Crossing experiments were performed on 2.5 cm Petri dishes seeded with OP50 *E. coli* food using one hermaphrodite *piwi* mutant at young adult stage together with ~5 wild type males. The efficiency of the cross was assessed by the % of F1 males present in the progeny. For each experiment, at least 5 crosses were set up and the best 3 were selected based on male incidence criteria. For each cross, 5 F1 hermaphrodite L4 larvae were transferred on individual plates and genotyped after egg laying to screen for heterozygous *piwi*/+ animals. F2 larvae from *piwi* heterozygote F1 were individually grown and genotyped to obtain wild type and *piwi* homozygous lines.

Brood size assays

Manually picked L1 larvae were grown individually on 2.5 cm Petri dishes seeded with OP50 *E. coli* food until adulthood and transferred on a new plate every 24 h for a total of three days. The brood size of each worm was scored by counting the total number of larvae laid on the three plates. For each brood size experiment, at least 15 worms were scored for each strain.

RNAi experiments

RNAi clones used in this study were obtained from the Ahringer library[54]. An empty vector (L4440) was used as a control in all our RNAi experiments. RNAi experiments for brood size assay were performed using manually picked L1 larvae grown on 2.5 cm Petri dishes seeded with bacteria producing dsRNA complementary to the gene of interest or control empty vector. RNAi experiments for RNA extraction were performed using 15 cm Petri dishes seeded with concentrated RNAi food.

RNA extraction

Synchronous populations of worms were grown at 20°C on NGM plates seeded with OP50 *E. coli* concentrated food at a density of maximum 40,000 animals per 15 cm Petri dish and harvested at Young Adult stage at 48 hours post hatching. The harvested animals were washed three times with M9 buffer and 40 μl of worm pellet was frozen in dry ice with TRI Reagent (MRC, Inc.). After five repetitions of freeze and thaw, total RNA was isolated according to the TRI Reagent protocol. Ten micrograms of RNA were treated with 2 U of Turbo DNase (Ambion) at 37°C for 30 minutes followed by phenol-extraction and isopropanol precipitation. Agilent 2200 TapeStation System was used to evaluate the RIN indexes of all the RNA preps, and only samples with RIN > 8 was used for downstream

applications. For the preparation of total RNA extracted from generation F4 of wild-type and *piwi* mutant worms 10 manually picked worms were used.

Strand-specific RNA sequencing (RNA-seq) library preparation

DNase-treated total RNA with RIN > 8 was used to prepare strand-specific RNA libraries. We developed an RNase H based method to degrade *C. elegans* and mitochondrial ribosomal RNAs (rRNAs) using 50nt oligos complementary to rRNA and mtRNA *C. elegans* sequences. The sequences of the oligos used are provided in Supplementary Table 4. 1 μg of DNase-treated total RNA was mixed with 1 μg of oligos at equimolar concentration and 1X probe hybridization buffer (200 mM NaCl, 10 mM Tris pH 7.5) and incubated in a thermocycler using the following parameters: 2 minutes at 95°C followed by 0.1°C/sec at 95-45°C, and 2 minutes hold at 45°C. Next 2 μl of Thermostable RNase H (epicentre) was added to the reactions together with 1X RNase H reaction buffer 50 mM Tris pH 7.5, 100 mM NaCl, 10 mM $MgCl_2$) and incubated for 30 minutes at 45°C. Next, digested RNAs were treated with 2 U of Turbo DNase (Ambion) at 37°C for 30 minutes followed by purification using 2.2 volumes of Agencourt RNAClean XP Beads (Beckman Coulter, NC0068576) following the manufacturer's instructions. 100 ng of Ribosomal-depleted RNAs were then used to generate strand-specific RNA libraries using NEBNext® Ultra™ II Directional RNA Library Prep Kit for Illumina® (E7760S). Multiplexed RNA libraries were quantified using Qubit Fluorometer High Sensitivity dsDNA assay kit (ThermoFisher, Q32851) and sequenced on NextSeq-500 Illumina platform using the NextSeq 500/550 High Output v2 kit 75 cycles (FC-404-2005).

Small RNA sequencing (sRNA-seq) library preparation

10 μg of total RNAs with RIN > 8 was used to generate small RNA libraries. The library preparation was performed as essentially described in[55], except that a 5' polyphosphatase (lucigen RP8092H) treatment was performed to be able to clone tri-phosphate small RNAs, and that the PAGE gel extraction after each ligation was substitute with purification by 1.8 volumes of Agencourt RNAClean XP Beads (Beckman Coulter, NC0068576) and 3 volumes of isopropanol. The multiplexed amplified libraries were further purified using PippinPrep DNA size selection with 3% gel cassettes and the following parameters for the selection: BP start (115) and the BP end (165). The purified libraries were quantified using Qubit Fluorometer High Sensitivity dsDNA assay kit (ThermoFisher, Q32851) and sequenced either on NextSeq-500 Illumina platform using the NextSeq 500/550 High Output v2 kit 75 cycles (FC-404-2005) or Illumina MiniSeq platform using MiniSeq High Output Reagent Kit 75-cycles (FC-420-1001).

Global run-on sequencing (GRO-seq)

GRO-seq experiments were performed as described in[56] except that biotin-UTP was used to label nascent RNAs. Two biological replicates were generated using synchronous 40,000 wild-type and *prg-1(n4357)* mutant worms harvested at 48 hours post hatching.

Immunoprecipitation for Co-IP or mass spectrometry experiments

Synchronous population of 120,000 (for CSR-1, PRG-1 IPs) or 40,000 (for WAGO-1 IPs for mass spectrometry) worms were harvested at 48 hours post hatching and suspended in the extraction buffer (50 mM HEPES pH7.5, 300 mM NaCl, 5 mM $MgCl_2$, 10% Glycerol, 0.25% NP40, protease inhibitor cocktails (Fermentas)) followed by 30 strokes using a metal dounce on ice. Crude protein extracts were centrifuged at 12,000 rpm at 4°C for 10 minutes. Protein concentration was quantified by the Bradford assay, and 2 mg of protein extract was incubated with 15 µl of packed Anti-FLAG M2 Magnetic Agarose Beads (Sigma M8823) for 1 hour at 4°C. After four washes with the extraction buffer the beads were resuspended with 2X NuPAGE LDS Sample Buffer (thermofisher) for Co-IP experiments or washed twice with 100 µL of 25 mM NH_4HCO_3 for mass spectrometry. For the Co-IP experiments shown in Fig. 4b and Extended Data Fig. 4e the total protein extract from *piwi* mutant and control strains were normalized on the level of CSR-1 protein to avoid differences in the total germline proteins due to the reduced germline tissue in *piwi* mutant.

Mass spectrometry

Digestion with 0.2 µg of trypsine/LysC (Promega) was performed on-beads derived from immunoprecipitation experiments for 1 hour in 100 µL of 25 mM NH_4HCO_3. Sample were then loaded onto a homemade C18 StageTips for desalting (principle by stacking one 3M Empore SPE Extraction Disk Octadecyl (C18) and beads from SepPak C18 CartridgeWaters into a 200 µl micropipette tip). Peptides were eluted using 40/60 MeCN/H_2O + 0.1% formic acid and vacuum concentrated to dryness. Online chromatography was performed with an RSLCnano system (Ultimate 3000, Thermo Scientific) coupled to an Orbitrap Fusion Tribrid mass spectrometer (Thermo Scientific). Peptides were trapped on a C18 column (75 µm inner diameter × 2 cm; nanoViper Acclaim PepMapTM 100, Thermo Scientific) with buffer A (2/98 MeCN/H_2O in 0.1% formic acid) at a flow rate of 4.0 µL/min over 4 min. Separation was performed on a 50 cm x 75 µm C18 column (nanoViper Acclaim PepMapTM RSLC, 2 µm, 100Å, Thermo Scientific) regulated to a temperature of 55°C with a linear gradient of 5% to 25% buffer B (100% MeCN in 0.1% formic acid) at a flow rate of 300 nL/min over 100 min. Full-scan MS was acquired in the Orbitrap analyzer with a resolution set to 120,000 and ions from each full scan were HCD fragmented and analyzed in the linear ion trap.

For identification the data were searched against the *Caenorhabditis elegans* (CAEEL) UP000001940 database using Sequest HF through proteome discoverer (version 2.1). Enzyme specificity was set to trypsin and a maximum of two missed cleavage site were allowed. Oxidized methionine, N-terminal acetylation, phosphorylated serine/threonine/tyrosine and carbamidomethyl cysteine were set as variable modifications. Maximum allowed mass deviation was set to 10 ppm for monoisotopic precursor ions and 0.6 Da for MS/MS peaks.

The resulting files were further processed using myProMS[57] v3.6 (work in progress). FDR calculation used Percolator and was set to 1% at the peptide level for the whole study. The label free quantification was performed by peptide Extracted Ion Chromatograms (XICs) computed with MassChroQ version 2.2.2[58]. For protein quantification, XICs from

proteotypic peptides shared between compared conditions (TopN matching) with missed cleavages and some modification (carbamidomethyl cysteines) were used. Global MAD normalization was applied on the total signal to correct the XICs for each biological replicate. To estimate the significance of the change in protein abundance, a linear model (adjusted on peptides and biological replicates) was performed and p-values were adjusted with a Benjamini–Hochberg FDR procedure with a control threshold set to 0.05. Cytoscape[59] was used to generate the interactome network map.

The mass spectrometry proteomics data have been deposited to the ProteomeXchange Consortium via the PRIDE[60] partner repository with the dataset identifier PXD012557.

Western blotting

Protein extracts, prepared as above, were resolved on precast NuPAGE™ Novex 4-12% Bis-Tris gels (Invitrogen NP0321BOX). The proteins were transferred to a nylon membrane with the semidry transfer Thermo Scientific™ Pierce™ Power System using the Pre-Programmed Method for High MW protein. The primary antibody used were α-PRG-1 antibody[6] (a gift from the Mello lab), α-CSR-1 antibody[61], α-PGL-1[62] and α-DEPS-1[38] (a gift from the Strome lab), α-FLAG (F3165, Sigma), α-GAPDH (Ab125247, Abcam), α-mCherry (RFP antibody [6G6], Chromotek), α-tubulin (Ab6160, Abcam), and the secondary antibody used were α-rabbit (31460, Pierce), α-mouse (31430, Pierce), or α-Rat (A9037, Sigma) HPR antibodies. The SuperSignal™ West Pico PLUS Chemiluminescent Substrate was used to detect the signal with the ChemiDoc™ MP imaging system (Biorad).

Confocal live imaging

Transgenic worms were mounted on 2% agarose pads in presence of 0.5% Sodium Azide. Confocal images were taken using ZEISS LSM 700 microscope with 40X objective or 63X objective for the H2B::mCherry quantification. Images were obtained using ZEISS ZEN microscope software and processed using ImageJ program V 2.0.0. The quantification of the histone H2B::mCherry was performed on a single confocal image taken at the surface of the pachytene region of the germline from 12 individual worms. In each worm, the H2B::mCherry fluorescent intensity was measured in 15 nuclei using Image J software. The incorporation of histone H2B::mCherry into the chromatin allows the visualization of chromosome compaction. Pachytene nuclei from wild-type and sterile *piwi* mutant animals were scored for lack of visible signs of chromosome compaction. The scored *piwi* mutant nuclei were still showing a diffused signal of histone H2B::mCherry in the nucleus. Nuclei with very low histone H2B::mCherry were excluded from the counting.

Immunostaining

Plates of adult worms were washed in PBS containing 0.1 % Tween (PBST). Ten worms were put on a polylysine coated slide in presence of 0.5% levamisole and the gonads were dissected on immobilized worms. The slide was fixed in 1 % paraformaldehyde for 5 minutes, frozen in liquid nitrogen and then immersed for at least 1 minute in methanol at -20°C. Slides were washed in PBST. The blocking was carried out in PBST, containing 0.5 % of Bovine Serum Albumine. Primary antibodies were diluted in PBST, containing 0.5 % of BSA and incubated over night at room temperature. Slides were washed at least 3 times

for 5 minutes in PBST 0.5 % BSA and secondary antibodies were added and incubated for 2 hours at room temperature. Slides were then washed for at least 2 times in PBST 0.5 % BSA and were counterstained with DAPI and mounted using Vectashield. The primary antibody used was α -FLAG (Sigma F1804) at dilution of 1:500 and the secondary antibody was goat anti-mouse (Invitrogen Alexa Fluor® 488) used at dilution 1:500.

RNA immunoprecipitation (RIP)

Synchronous population of 40,000 worms were harvested at 48 hours post hatching and suspended in the extraction buffer (50 mM HEPES pH7.5, 300 mM NaCl, 5 mM $MgCl_2$, 10% Glycerol, 0.25% NP40, protease inhibitor cocktails (Fermentas)) followed by 30 strokes using a metal dounce on ice. Crude protein extracts were spun at 12,000 rpm at 4°C for 10 minutes. Protein concentration was quantified by the Bradford assay, and 1 mg of protein extract was incubated with 15 µl of packed Anti-FLAG M2 Magnetic Agarose Beads (Sigma M8823) for 1 hour at 4°C. After four washes with extraction buffer, the immunoprecipitated protein was eluted twice with 100 µL of 3XFLAG peptide (Sigma F4799) for 30 minutes at 4°C. Next, the eluate was incubated with 750 µL of TRI Reagent (MRC, Inc.) to extract the immunoprecipitated RNAs. 750 µL of TRI Reagent (MRC, Inc.) was also added to 10% of protein extract before the immunoprecipitation (Input). The extracted RNAs were then analyzed by RT-qPCR to quantify mRNAs or used to clone small RNAs.

RT-qPCR

1 µg of DNase-treated total RNA was used as a template to generate cDNA, using random hexamer primers and M-MLV Reverse Transcriptase and the qPCR reactions were performed using Applied Biosystems Power up SYBR Green PCR Master mix following the manufacturer's instructions using the Applied Biosystems™ QuantStudio™ 3 Real-Time PCR System. The primers used for the qPCR are available in Supplementary Table 5.

Chromatin Immunoprecipitation (ChIP)

Procedures were as described in[9] with the following modification. We harvested eggs by hypochlorite treatment, and synchronous populations of worms were grown for 48 hours post-hatching at 20ºC on OP-50 *E. coli* at a density of approximately 40,000 animals per 15cm Petri dish. Approximately 2 mg of protein chromatin extract was used for each ChIP experiment. The RFP-Trap® coupled to agarose beads (Chromotek) was used for the immunoprecipitation of the chromatin extracts and performed for 2h at 4°C. The primers used for the qPCR are available in Supplementary Table 5.

Sequencing data analyses

RNA-seq—Multiplexed Illumina sequencing data was demultiplexed using Illumina bcl2fastq converter (version v2.17.1.14). The read quality of all the libraries were assessed using fastQC (version v0.11.5). Fastq reads were aligned on *C. elegans* genome (ce11, *C. elegans* Sequencing Consortium WBcel235) using HISAT2 version 2.0.4[63] with the default settings. After the alignment on *C. elegans* genome, featureCounts version 1.5.2[64] was used for counting reads mapped to annotated genomic features such as protein-coding genes,

pseudogenes, RNA transposons, DNA transposons, simple repeats, satellites, ribosomal RNAs (rRNAs), transfer RNAs (tRNAs), small nuclear RNAs (snRNAs), small nucleolar RNAs (snoRNAs), antisense RNAs. Annotations were obtained from Ensembl release 81 as distributed in the Illumina iGenomes collection, with the exception of repetitive sequences, which were taken from the repeatMasker annotation file present in the UCSC genome annotation database for the Feb. 2013 (WBcel235/ce11) assembly of the *C. elegans* genome. Counted reads for each genomic feature were used for differential expression analysis using the R/Bioconductor package DESeq2 version 1.20.0[65]. Up-regulated and down-regulated genes are detected based on the differential expression criteria of adjusted p-value < 0.05 and at least two-fold increase/decrease in expression levels in relation to the control samples.

sRNA-seq—Multiplexed Illumina sequencing data was demultiplexed using Illumina bcl2fastq converter (version v2.17.1.14). The read quality of all the libraries were assessed using fastQC. The 3' adaptor was trimmed from raw reads using Cutadapt version 1.15[66] with the following parameter -a TGGAATTCTCGGGTGCCAAGG --discard-untrimmed. 5' and 3' end Unique Molecular Identifier (UMI) were used to deduplicate the trimmed reads. Deduplication was performed by first sorting reads by sequence using option -s of fastq-sort (from fastq-tools version 0.8: https://github.com/dcjones/fastq-tools/tree/v0.8) and then using a custom Haskell program that kept the best quality at each position among reads of identical sequence. 4 nt UMI were then trimmed at both ends using Cutadapt (options -u 4 and -u -4). Finally, we selected only deduplicated reads ranging from 18 to 26 nt using bioawk (https://github.com/lh3/bioawk). The selected 18-26 nt reads were aligned on *C. elegans* genome (ce11, *C. elegans* Sequencing Consortium WBcel235) using Bowtie2 version 2.3.4.1[67] with the following parameters -L 6 -i S,1,0.8 -N 0. A custom Python script was used to classify reads into small RNA categories, based on the known annotations at their mapping positions, their orientation with respect to these annotations, and their length and starting nucleotide. Annotation sources were the same as for RNA-seq analyses. Roughly, reads matching piRNA (allowing up to 26 nt to account for the possible presence of not completely matured piRNAs) or miRNA annotations were classified as such. 21-23 nt reads that were not classified as piRNAs or miRNAs and that started with G were classified as potential 22G-RNAs and further classified into sub-categories based on them being antisense to protein-coding genes, pseudogenes, RNA transposons, DNA transposons, simple repeats, or satellites. We call the set of all these antisense 22G-RNAs "si 22G". Reads per million (RPM) were calculated by dividing the reads counts by the total number of reads less structural RNAs, i.e. sense small RNA reads likely derived from degraded ribosomal RNAs (rRNAs), transfer RNAs (tRNAs), small nuclear RNAs (snRNAs), small nucleolar RNAs (snoRNAs), as estimated by running featureCounts on the mapped 18-26 nt reads, and multiplied per 1,000,000. Next, $\log_2$ fold changes were calculated for each replicate, adding 0.25 RPM as "pseudo-counts", and the mean value across replicates was used. For immunoprecipitation (IP) experiments, we calculated the RPM of the reads from input and from IP. Next, we calculated the $\log_2$ fold changes between IP versus input. Small RNAs from genes with $\log_2$ fold changes ≥1 in IP versus input were considered to be associated with the immunoprecipitated AGO protein.

GRO-seq—Multiplexed Illumina sequencing data was demultiplexed using Illumina bcl2fastq converter (version v2.17.1.14). The read quality of all the libraries were assessed using fastQC. The 3' adaptor was trimmed from raw reads using Cutadapt (option -a TGGAATTCTCGGGTGCCAAGG). Only reads with at least 24 nt after trimming (but including 5' and 3' randomized tetramers) were kept (option -m 24). Reads in which the adaptor was not found were also kept (option --untrimmed-output). 5' and 3' end tetramers were removed using Cutadapt (options -u 4 and -u -4). The reads were aligned on *C. elegans* genome (ce11, *C. elegans* Sequencing Consortium WBcel235) using Bowtie2 with the default parameters. After the alignment on *C. elegans* genome, read counting with featureCounts and differential expression analysis with DESeq2 were performed the same way as for RNA-seq data, with the same criteria to detect up-regulated and down-regulated genes.

Generation of bigwig files—For all library types, normalized bigwig files were generated from the mapping results using millions of non-structural mappers as normalization factor. This normalized coverage information was computed on 10 bp bins using the bedtools[68] and bedops version 2.4.26[69] packages.

Comparison between RNA-seq (or GRO-seq) and sRNA-seq—For the comparison between RNA-seq (or GRO-seq) and sRNA-seq, plots were generated by plotting log fold changes in the DESeq2 analysis of the RNA-seq (or GRO-seq) data against the RPM fold of the "si_22G" sRNA category using custom Python scripts.

Metaprofile—Metaprofiles were generated using RPM from small RNA-seq analysis by summarizing normalized coverage information (taken from bigwig files and averaged across replicates) along histone genes or 200nt upstream and downstream of the stem-loop structure of histone mRNAs using the deeptools package version 3.1.2[70].

Gene lists

The gene lists used are provided in Supplementary Table 6.

Statistics and reproducibility

Almost all experiments shown in this study were performed independently at least two times and no inconsistent results were observed. All attempts at replication were successful. Immunoprecipitation and mass spectrometry experiments were conducted with four biological replicates. All the RNA sequencing experiments has been performed using two biological replicates. For details of the particular statistical analyses employed, precise P values, statistical significance and sample sizes for all graphs, see Figure legends and Methods. The source data for Figs. 1,2,3,4,5,6 and Extended Data Figs. 1,2,3,4,5,6 have been provided.

Extended Data

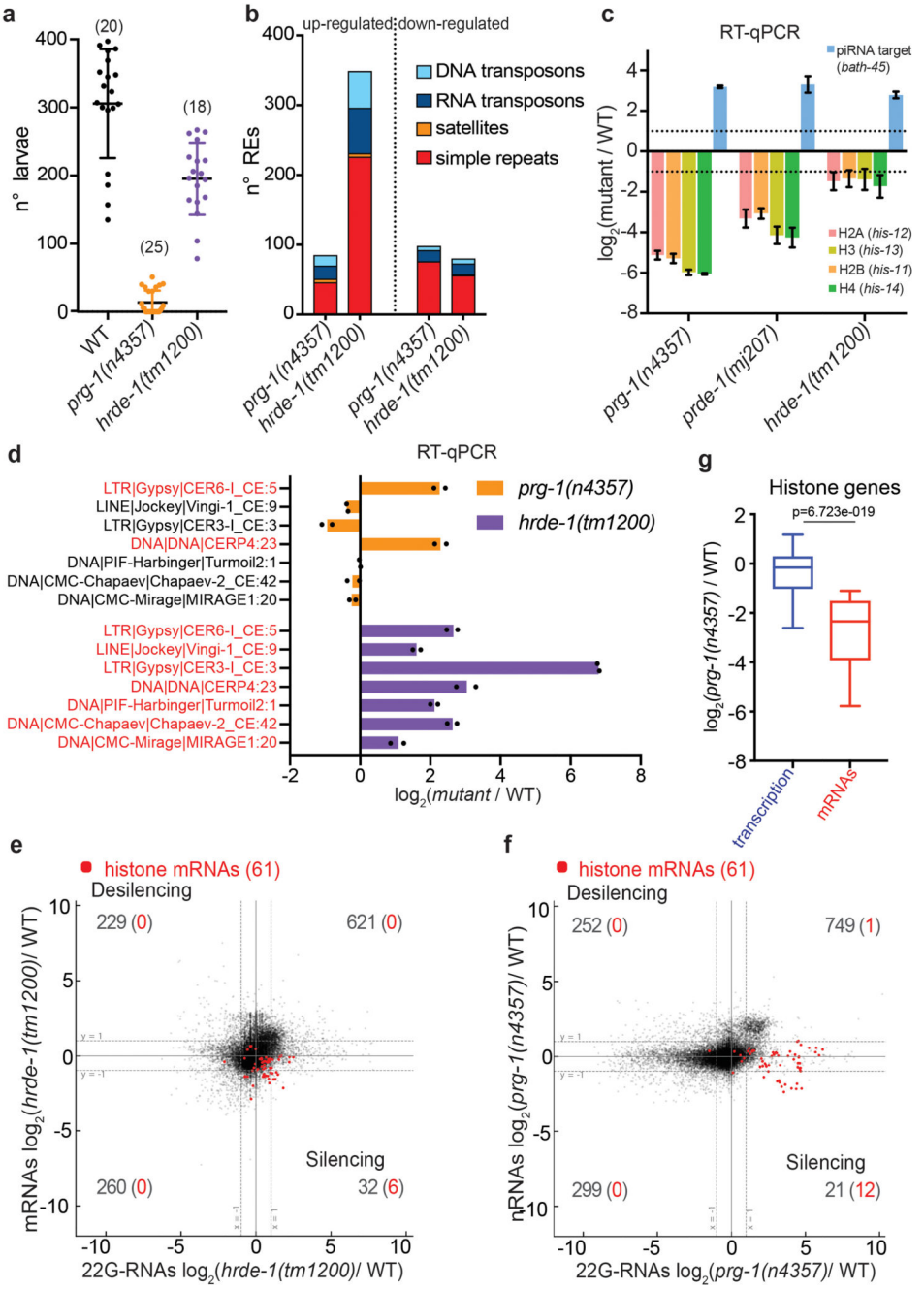

Extended Data Fig. 1. Histone silencing occurs at the post-transcriptional level only in mutants of the piRNA biogenesis pathway

a, Brood size assay of wild-type, *prg-1 (n4357)* and *hrde-1 (tm1200)* mutant worms as in Fig. 1d. The black lines indicate the mean, the error bars the standard deviation, and the n (animals) is indicated above in parenthesis. **b**, Number of individual misregulated REs by RNA-seq (≥ 2-fold and padj < 0.05, Wald test) in *piwi* or *hrde-1* mutants. Data shown represent average of two biologically independent replicates. **c**, RT-qPCR $\log_2$ fold change of histone mRNAs and piRNA-dependent 22G-RNA targets in *prg-1 (n4357), prde-1*

Europe PMC Funders Author Manuscripts

(mj207), and hrde-1 (tm1200) mutants compared to wild-type worms. The bars indicate the mean and error bars indicate the standard deviation. n = 3 biologically independent experiments. **d**, RT-qPCR showing $\log_2$ fold change of individual DNA or RNA transposons in mutant vs. wild-type. Up-regulated transposons by RNA-seq are labelled in red. The bars indicate the mean and the black dots individual data from two biologically independent experiments. **e**, mRNA $\log_2$ fold change (y axis) and 22G-RNA $\log_2$ fold change (x axis) in *hrde-1(tm1200)* mutant vs. wild-type worms for protein-coding genes as in Fig. 1a. Wald test was used to calculate the p value. Data shown represent average of two biologically independent replicates. **f**, nascent RNA (nRNA) $\log_2$ fold change (y axis) and 22G-RNA $\log_2$ fold change (x axis) in *prg-1 (n4357)* mutant vs. wild-type worms for protein-coding genes. Red dots indicate the replicative histone genes. Wald test was used to calculate the p value. Data shown represent average of two biologically independent replicates. **g**, Box plot showing transcriptional (GRO-seq) and post-transcriptional (RNA-seq) histone gene expression changes in *prg-1 (n4357)* mutant vs. wild-type worms. The median (line), first and third quartiles (box), and whiskers (5th and 95th percentile) are shown. Two-tailed p value calculated with the Mann-Whitney-Wilcoxon tests is shown, using the sample size n (number of genes) = 61. Source data are available in Source Data Extended Data Fig. 1.

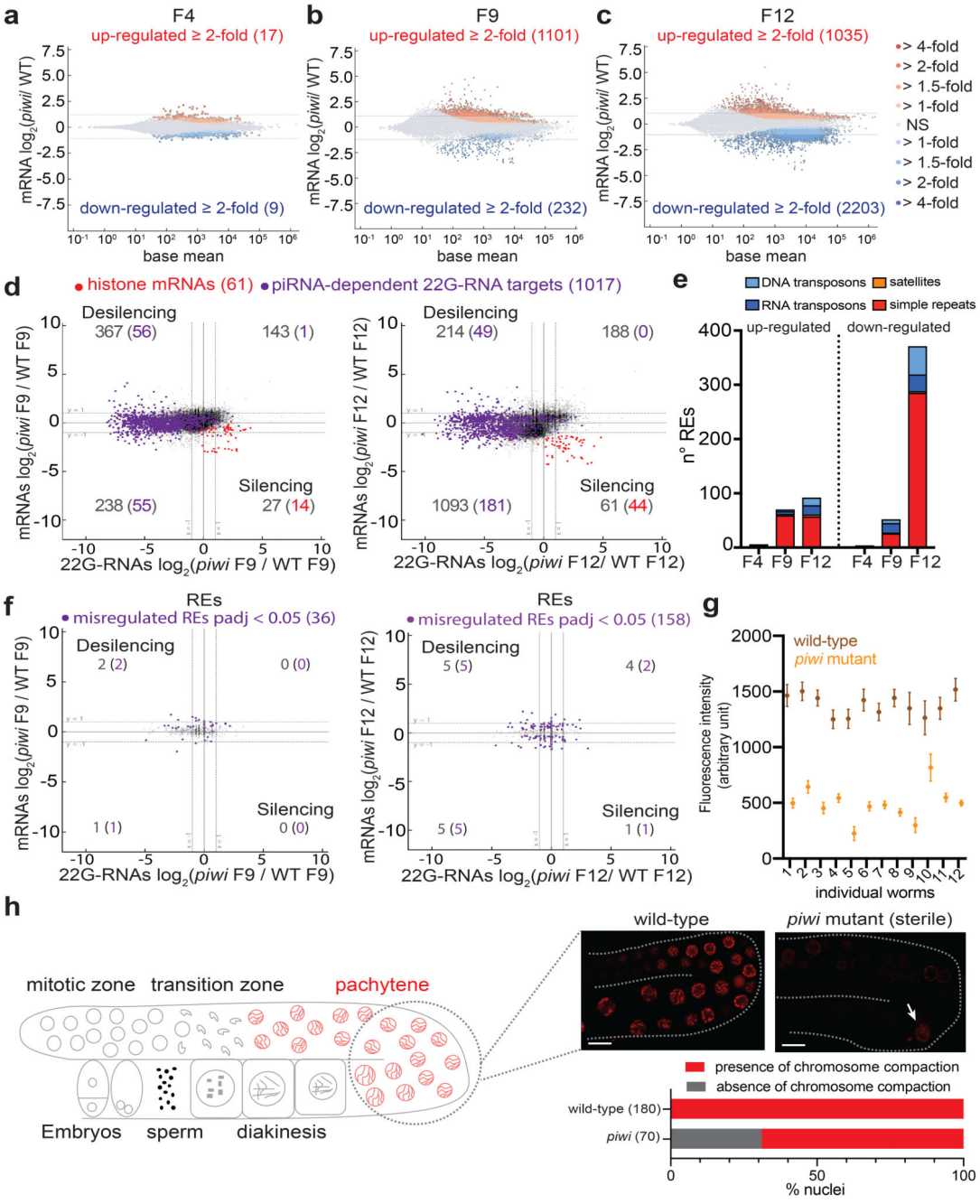

Extended Data Fig. 2. Transgenerational gene expression changes of protein-coding genes and REs in *piwi* mutant

a, b, c, MA-plot showing mRNA $\log_2$ fold change between *piwi* mutant and wild-type lines at different generations. Red and blue dots correspond to significant $\log_2$ fold change (padj < 0.05, Wald test). The number in parenthesis indicates the number of misregulated genes ≥ 2-fold. The average from two biologically independent replicates is shown. **d**, Comparison between mRNA $\log_2$ fold change (y axis) by and 22G-RNA $\log_2$ fold change (x axis) as shown in Fig. 1a using *piwi* mutant and wild-type CRISPR-Cas9 lines at F9 (left) and F12

Europe PMC Funders Author Manuscripts

(right). **e**, Plot showing the number of individual up-regulated and down-regulated REs by RNA-seq (padj < 0.05, Wald test) in *piwi* mutant compared to wild-type CRISPR-Cas9 lines at F4, F9, and F12. Only uniquely mapped reads were considered for this analysis. Data shown represent average of two biologically independent replicates. **f**, Comparison between RNA $\log_2$ fold change (y axis) by and 22G-RNA $\log_2$ fold change (x axis) as shown in Fig. 1a using *piwi* mutant and wild-type CRISPR-Cas9 lines at F9 (left) and F12 (right). Significant misregulated RE families are indicated (padj < 0.05, Wald test). The average from two biologically independent replicates is shown. **g**, Average and standard deviation of H2B::mCherry quantification in 15 pachytene nuclei in each individual wild-type and *piwi* mutant worm. n = 15 animals. **h**, Visualization of chromosome compaction in pachytene nuclei using H2B::mCherry wild-type and *piwi* mutant worms. The arrow indicates an example of nucleus with defective chromosome compaction in sterile piwi mutant. The percentage of nuclei lacking chromosome compaction in piwi mutant is shown below the images and the number in parenthesis indicates the number of nuclei counted. The white bars indicate 20 μM size. The experiment was repeated twice with similar results. Statistical source data are available in Source Data Extended Data Fig. 2.

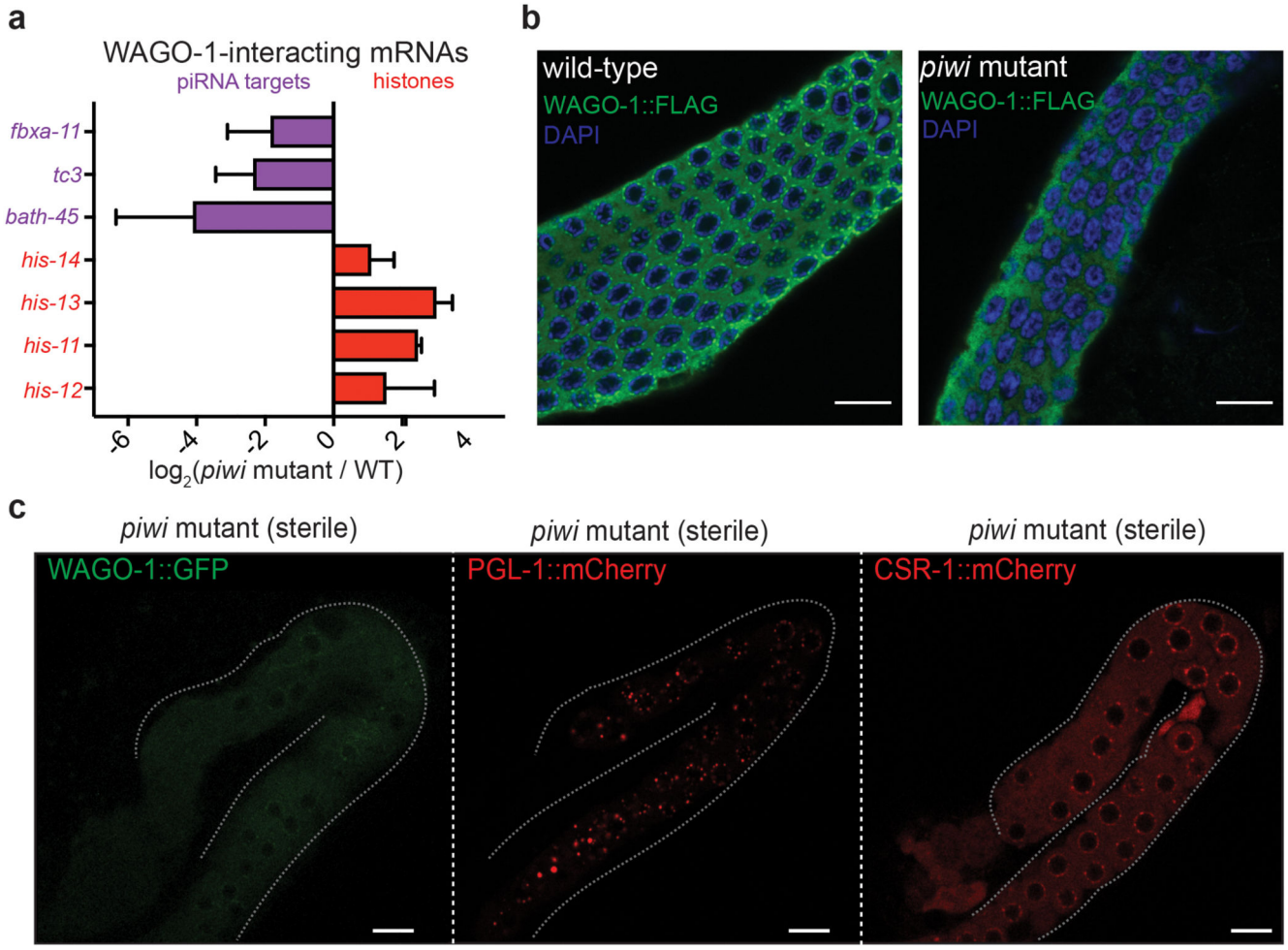

Extended Data Fig. 3. WAGO-1 relocalize from piRNA targets to histone mRNAs

a, RNA immunoprecipitation (RIP) experiments followed by RT-qPCR showing the $\log_2$ fold change of the WAGO-1-interacting mRNAs in *piwi* mutant vs. wild-type worms. The bars indicate the mean and error bars indicate the standard deviation. n = 4 biologically independent experiments. **b**, Co-IP experiments showing CSR-1 interactions with WAGO-1 in wild-type and *piwi* mutant worms. Presence (+) or absence (-) of the tagged proteins or *piwi* mutation are indicated. Immunoprecipitation was performed using α-FLAG antibody, and the blots were probed with α-CSR-1 or α-FLAG antibodies. **c**, Immunostaining with α-FLAG antibody showing WAGO-1::FLAG localization in wild-type and *piwi* mutant (green signal). DAPI signal is shown in blue. The white bars indicate 20μM size. The experiment was repeated independently twice with similar results. **d**, Live confocal images of WAGO-1::GFP, PGL-1::mCherry, and CSR-1::mCherry in sterile *piwi* mutant germlines. The white bars indicate 10μM size. The experiment was repeated independently three times with similar results. Source data are available in Source Data Extended Data Fig. 3.

Europe PMC Funders Author Manuscripts

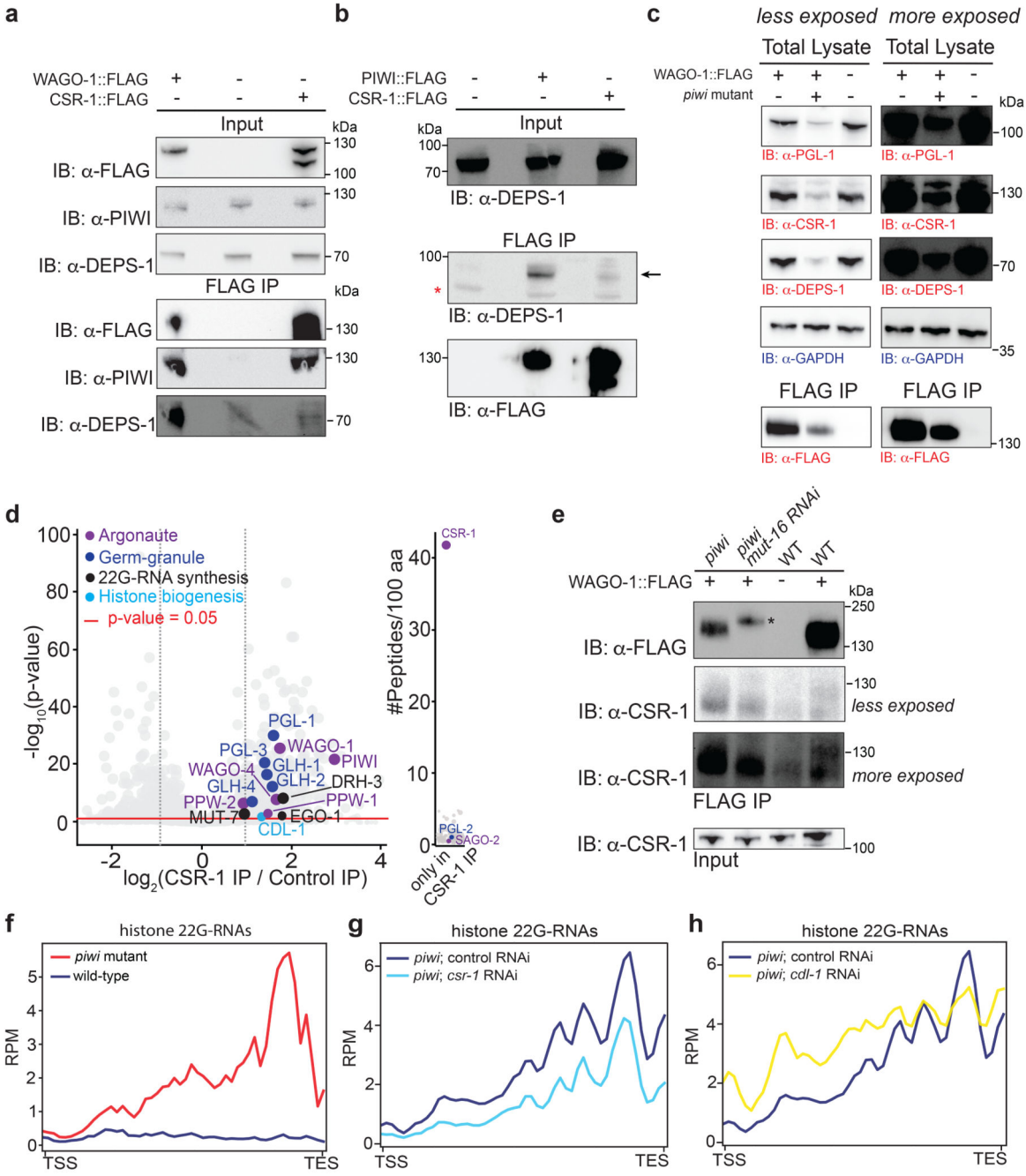

Extended Data Fig. 4. CSR-1 and CDL-1 contribute to the biogenesis of histone 22G-RNAs in piRNA mutant

a, Co-IP experiments using α-FLAG antibody for IPs and α-PIWI, α-DEPS-1 or α-FLAG antibodies for blots. Presence (+) or absence (-) of the FLAG tagged proteins are indicated. The experiment was repeated independently twice with similar results. **b**, Co-IP experiments as in **a**, showing DEPS-1 interaction with PIWI and not with CSR-1. The blots were probed with α-DEPS-1 or α-FLAG antibodies. The experiment was repeated independently twice with similar results. **c**, Immunoblot showing CSR-1, PGL-1, DEPS-1, GAPDH from total

protein lysate or FLAG immunoprecipitation in WT and *piwi* mutant worms. Blots for germline-enriched and ubiquitous proteins are shown in red and blue respectively. The experiment was repeated independently twice with similar results. **d**, Volcano plot showing enrichment values and corresponding significance levels for proteins co-purifying with CSR-1 (see also Supplementary Table 1c). Argonaute proteins, germ granule components, 22G-RNA and histone biogenesis factors are indicated. The size of the dots is proportional to the number of peptides used for the quantification. The linear model was used to compute protein quantification ratio and the red horizontal line indicates the two-tailed p value = 0.05. n = 4 biologically independent experiments. **e**, Co-IP experiments as in **a**, showing CSR-1 interaction with WAGO-1 in wild-type, *piwi* mutant and *piwi* mutant treated with *mut-16* RNAi. The blots were probed with α-CSR-1 or α-FLAG antibodies. * The higher migration of this band is due by the GFP fused to WAGO-1::FLAG in this strain. The experiment was repeated independently twice with similar results. **f, g, h**, Metaprofile analysis showing the distribution of normalized 22G-RNA reads (RPM) across histone genes in wild-type (blue line), *piwi* mutant (red line), and *piwi* mutant animals treated with control RNAi (blue line), *csr-1* RNAi (light blue line) or *cdl-1* RNAi (yellow line). The experiment was repeated independently twice with similar results. Statistical source data and unprocessed blots are available in Source Data Extended Data Fig. 4.

Europe PMC Funders Author Manuscripts

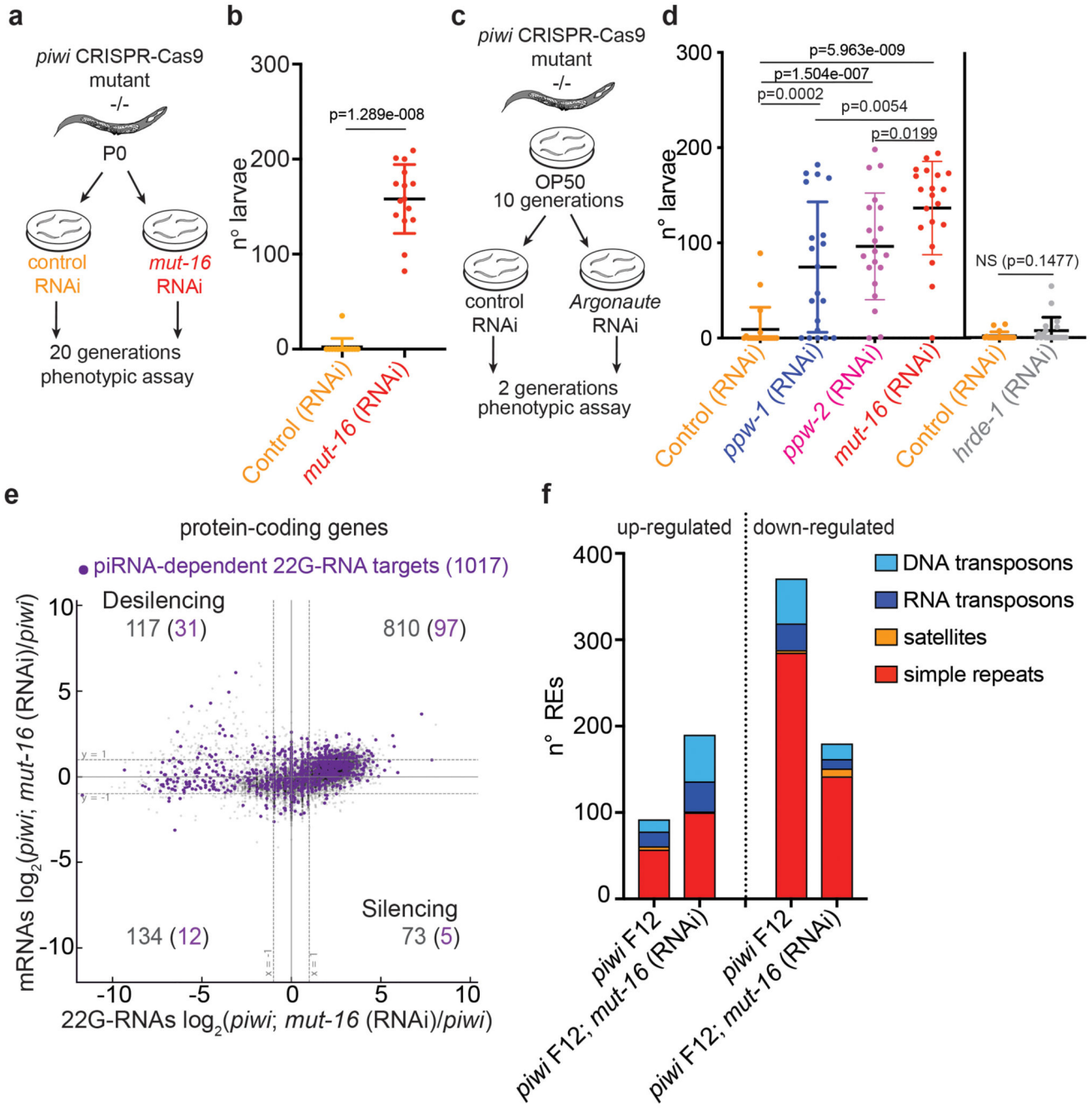

Extended Data Fig. 5. Depletion of MUT-16, PPW-1, PPW-2 and not HRDE-1 restores fertility in *piwi* mutant independently of REs silencing

a, Schematic of the RNAi experiment using CRISPR-Cas9 *piwi* mutant worms grown immediately on plates seeded with *E. coli* expressing dsRNA targeting *mut-16* or empty vector for 20 generations. **b**, Results from the experiments described in **a**. Each dot corresponds to the number of alive larvae from individual worms. The black lines indicate the mean and the error bars the standard deviation. Two-tailed p value calculated using the Mann-Whitney-Wilcoxon tests is shown. n = 15 animals. **c**, Schematic of the RNAi

experiment using CRISPR-Cas9 *piwi* mutant worms grown for 10 generations on plates seeded with *E. coli* OP50 (standard maintenance food) and then shifted for two generations on plates seeded with *E. coli* expressing dsRNA targeting *hrde-1, ppw-1, ppw-2, mut-16* or empty vector. **d**, Results from brood size assay of the experiment described in **c**. The brood size assay is performed as in **b**. *hrde-1* RNAi and its own control has been performed independently from the other RNAi treatment. The black lines indicate the mean and the error bars the standard deviation. Two-tailed p value calculated using the Mann-Whitney-Wilcoxon tests is shown. n = 20 animals. **e**, Comparison similar to the one showed in Fig. 1a between mRNA $\log_2$ fold change (y axis) and 22G-RNA $\log_2$ fold change (x axis) in *piwi* mutant animals treated with *mut-16* RNAi compared to control RNAi for protein-coding genes. Purple dots indicate the piRNA-dependent 22G-RNA targets. **f**, Plot showing the number of up-regulated and down-regulated individual REs by RNA-seq (padj < 0.05, Wald test) in *piwi* mutant animals treated with control or *mut-16* RNAi. Only uniquely mapped reads were considered for this analysis. Data shown represent average of two biologically independent replicates. Source data available in Source Data Extended Data Fig. 5.

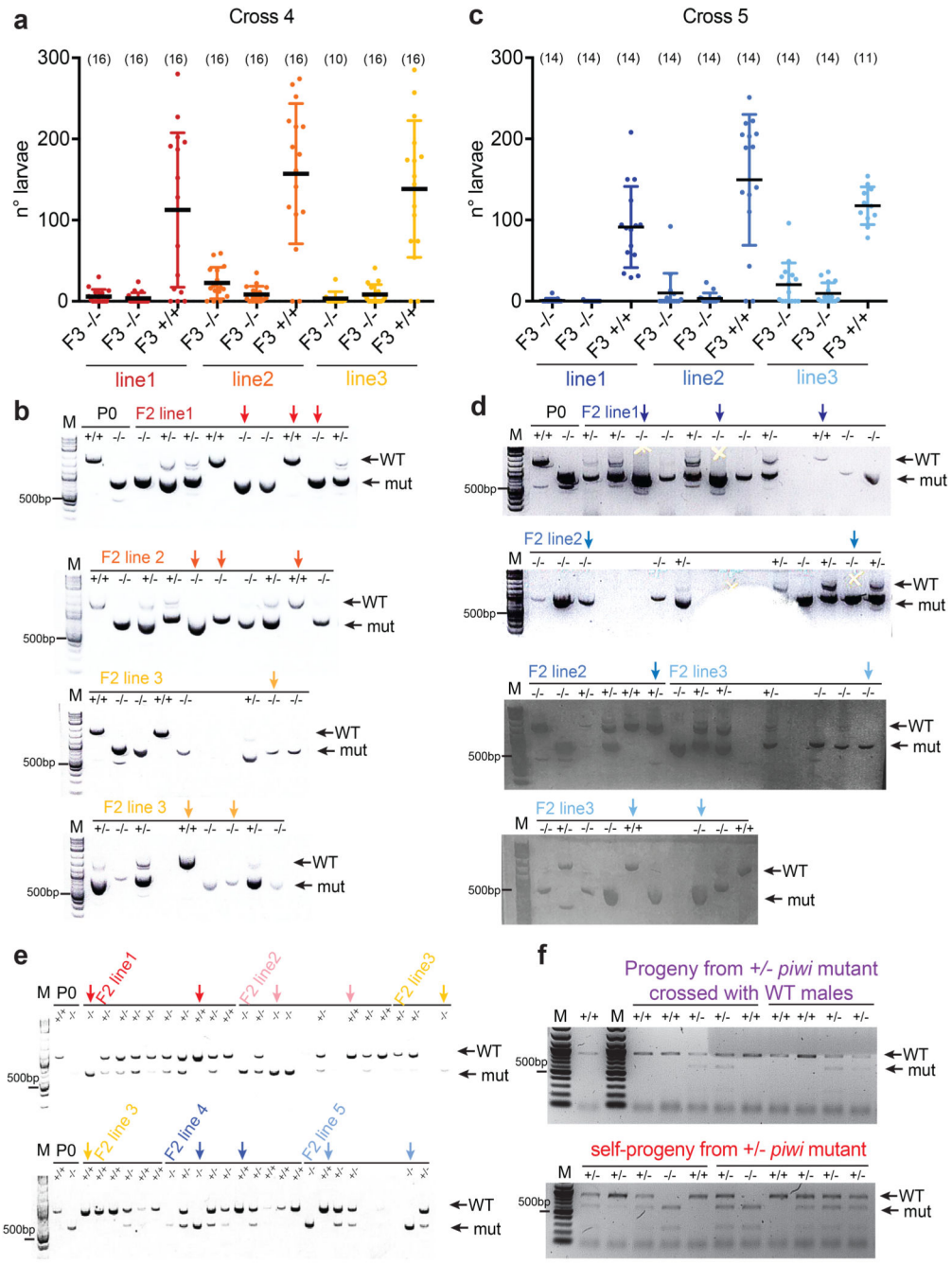

Extended Data Fig. 6. Decreased fertility in wild-type worms after crossing with piRNA mutants

a, Brood size assay similar to the one showed in Fig. 6b of the outcross experiment described in Fig. 6a. One wild-type and two *piwi* mutants were selected from independent F2 heterozygote lines from cross number 4. The black lines indicate the mean, the error bars the standard deviation, and the n (animal number analyzed) is indicated in parenthesis. **b**, Genotyping results by electrophoresis gel analysis of the F3 lines derived from self-crossed F2 heterozygote lines. Genomic DNA were extracted from individual animals after they released their progeny and a region spanning *prg-1* mutation was amplified by PCR and

Europe PMC Funders Author Manuscripts

digested with a restriction enzyme. The expected mutant and wild-type pattern of digestion is indicated by the black arrows compared to the marker (M). The selected wild-type and *piwi* mutant F3 lines are indicated by arrows with different colors corresponding to the colors used in the brood size assay shown in **a**. The experiment was repeated independently twice with similar results. **c,** same analysis as in **a,** performed with the crossing experiment number 5. The black lines indicate the mean, the error bars the standard deviation, and the sample size (n) is indicated in parenthesis. **d,** same analysis as in **b**, performed with the crossing experiment number 5. The experiment was repeated independently twice with similar results. White cross marks in the upper two panels indicate some of the selected lines used) **e**, Genotyping results similar to the one described in **b** using F3 lines derived from the crossing experiment between CRISPR-Cas9 *piwi* mutant hermaphrodite and wild-type males. The experiment was repeated independently twice with similar results. **h**, Genotyping results similar to the one described in **b**. The experiment was repeated independently twice with similar results. Statistical source data are available in Source Data Extended Data Fig. 6.

Europe PMC Funders Author Manuscripts

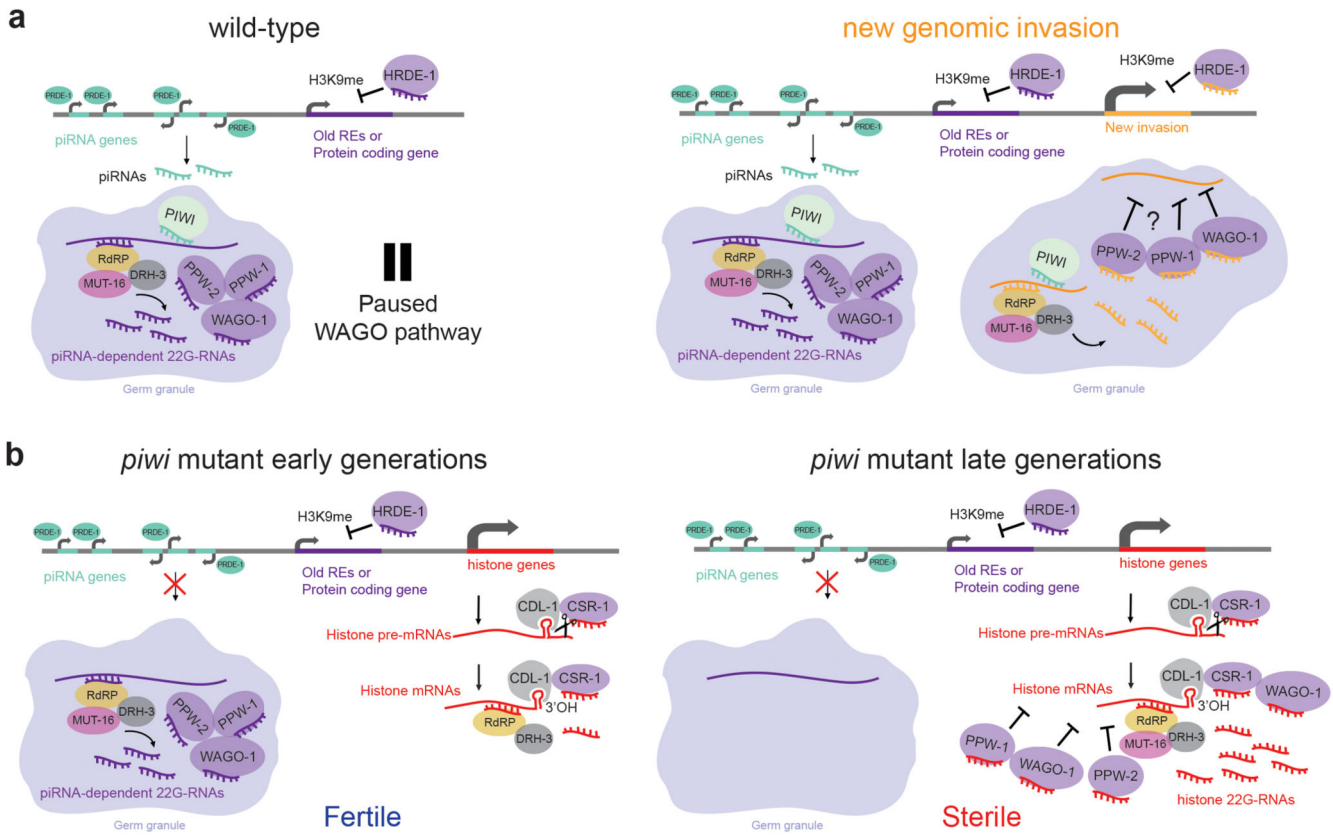

Extended Data Fig. 7. Model illustrating the molecular consequences in animals losing piRNAs.

a, PRDE-1 promotes the transcription of piRNAs from thousands of genomic loci. piRNAs are then loaded into PIWI, which triggers the biogenesis of WAGO-bound 22G-RNAs from thousands protein-coding genes and REs and keep the WAGO pathway in a paused state (left). In case of new genomic invasions, the piRNAs and WAGOs machineries promptly silence new REs at the transcriptional and the post-transcriptional levels (right). REs can be kept silenced at the chromatin level by H3K9 methyl transferases in a piRNA-dependent or piRNA-independent manner. **b**, In early generations of piRNA mutants (left), the PIWI-induced silencing complex is still maintained on piRNA targets thanks to the interaction with germ granule components. In late generations (right), the piRNA-induced silencing complex is disrupted and some of its components, including WAGO-1, relocalize to the cytoplasm where it interacts with CSR-1 on histone mRNAs to synthesize antisense 22G-RNAs in a CSR-1-dependent manner (right). The PIWI, the WAGO and the CSR-1 pathways share interactions with many RNAi factors and germ granule components in wild-type worms, and in late generations of *piwi* mutants WAGO-1 and possibly PPW-1 and PPW2 become preferentially loaded by CSR-1-dependent histone 22G-RNAs to silence histone mRNAs, which lead to sterility. We propose that the histone mRNA silencing acts as an evolutionary force to maintain a constant production of piRNAs ready to silence new genomic invasion.

Europe PMC Funders Author Manuscripts

Supplementary Material

Refer to Web version on PubMed Central for supplementary material.

Acknowledgements

We thank the members of the Cecere laboratory, Daniele Canzio, Nicola Iovino, Ritwick Sawarkar and Peter Andersen for helpful discussions on the manuscript. We thank the Miska, the Mello, the Kennedy, the Seydoux, the Claycomb, the Strome, and the Dumont laboratories for sharing strains and/or antibodies. Some strains were provided by the CGC, funded by NIH Office of Research Infrastructure Programs (P40 OD010440). This project has received funding from the Institut Pasteur, the CNRS, and the European Research Council (ERC) under the European Union's Horizon 2020 research and innovation programme under grant agreement No ERC-StG-679243. G.B. is part of the Pasteur - Paris University (PPU) International PhD Program and has received funding from the European Union's Horizon 2020 research and innovation programme under the Marie Sklodowska-Curie grant agreement No 665807. E.C. was supported by a Pasteur-Cantarini Fellowship program. F.D. and D.L. has received funding from “Région Ile-de-France” and Fondation pour la Recherche Médicale grants to support this study.

References

1. Ozata DM, Gainetdinov I, Zoch A, O’Carroll D, Zamore PD. PIWI-interacting RNAs: small RNAs with big functions. Nature Reviews Genetics. 2019; doi: 10.1038/s41576-018-0073-3
2. Thomson T, Lin H. The Biogenesis and Function of PIWI Proteins and piRNAs: Progress and Prospect. Annu Rev Cell Dev Biol. 2009; doi: 10.1146/annurev.cellbio.24.110707.175327
3. Tóth KF, Pezic D, Stuwe E, Webster A. The pirna pathway guards the germline genome against transposable elements. Advances in Experimental Medicine and Biology. 2016; doi: 10.1007/978-94-017-7417-8_4
4. Wu P-H, et al. An Evolutionarily Conserved piRNA-producing Locus Required for Male Mouse Fertility. bioRxiv. 2018; doi: 10.1101/386201
5. Gou LT, et al. Ubiquitination-Deficient Mutations in Human Piwi Cause Male Infertility by Impairing Histone-to-Protamine Exchange during Spermiogenesis. Cell. 2017; doi: 10.1016/j.cell.2017.04.034
6. Simon M, et al. Reduced Insulin/IGF-1 Signaling Restores Germ Cell Immortality to Caenorhabditis elegans Piwi Mutants. Cell Rep. 2014; doi: 10.1016/j.celrep.2014.03.056
7. Katz DJ, Edwards TM, Reinke V, Kelly WG. A C. elegans LSD1 Demethylase Contributes to Germline Immortality by Reprogramming Epigenetic Memory. Cell. 2009; doi: 10.1016/j.cell.2009.02.015
8. Buckley BA, et al. A nuclear Argonaute promotes multigenerational epigenetic inheritance and germline immortality. Nature. 2012; doi: 10.1038/nature11352
9. Frézal L, Demoinet E, Braendle C, Miska E, Félix M-A. Natural Genetic Variation in a Multigenerational Phenotype in C. elegans. Curr Biol. 2018; 28:2588–2596.e8. [PubMed: 30078564]
10. Spracklin G, et al. Identification and Characterization of C. elegans RNAi Inheritance Machinery. Genetics. 2017; :1–19. DOI: 10.20944/preprints201702.0096.v1
11. Perez MF, Lehner B. Intergenerational and transgenerational epigenetic inheritance in animals. Nat Cell Biol. 2019; 21:143–151. [PubMed: 30602724]
12. Batista PJ, et al. PRG-1 and 21U-RNAs Interact to Form the piRNA Complex Required for Fertility in C. elegans. Mol Cell. 2008; doi: 10.1016/j.molcel.2008.06.002
13. Ruby JG, et al. Large-Scale Sequencing Reveals 21U-RNAs and Additional MicroRNAs and Endogenous siRNAs in C. elegans. Cell. 2006; doi: 10.1016/j.cell.2006.10.040
14. Das PP, et al. Piwi and piRNAs Act Upstream of an Endogenous siRNA Pathway to Suppress Tc3 Transposon Mobility in the Caenorhabditis elegans Germline. Mol Cell. 2008; doi: 10.1016/j.molcel.2008.06.003
15. Cecere G, Zheng GXY, Mansisidor AR, Klymko KE, Grishok A. Promoters Recognized by Forkhead Proteins Exist for Individual 21U-RNAs. Mol Cell. 2012; 47:734–745. [PubMed: 22819322]

16. Gu W, et al. CapSeq and CIP-TAP identify pol ii start sites and reveal capped small RNAs as C. elegans piRNA precursors. Cell. 2012; doi: 10.1016/j.cell.2012.11.023
17. Shen EZ, et al. Identification of piRNA Binding Sites Reveals the Argonaute Regulatory Landscape of the C. elegans Germline. Cell. 2018; doi: 10.1016/j.cell.2018.02.002
18. Zhang D, et al. The piRNA targeting rules and the resistance to piRNA silencing in endogenous genes. Science (80-.). 2018; doi: 10.1126/science.aao2840
19. Lee HC, et al. C. elegans piRNAs mediate the genome-wide surveillance of germline transcripts. Cell. 2012; doi: 10.1016/j.cell.2012.06.016
20. Bagijn MP, et al. Function, targets, and evolution of Caenorhabditis elegans piRNAs. Science (80-.). 2012; doi: 10.1126/science.1220952
21. Houri-Ze'evi L, et al. A Tunable Mechanism Determines the Duration of the Transgenerational Small RNA Inheritance in C. elegans. Cell. 2016; doi: 10.1016/j.cell.2016.02.057
22. Spracklin G, et al. The RNAi inheritance machinery of caenorhabditis elegans. Genetics. 2017; doi: 10.1534/genetics.116.198812
23. Wan G, et al. Spatiotemporal regulation of liquid-like condensates in epigenetic inheritance. Nature. 2018; doi: 10.1038/s41586-018-0132-0
24. Zeller P, et al. Histone H3K9 methylation is dispensable for Caenorhabditis elegans development but suppresses RNA:DNA hybrid-associated repeat instability. Nat Genet. 2016; doi: 10.1038/ng.3672
25. McMurchy AN, et al. A team of heterochromatin factors collaborates with small RNA pathways to combat repetitive elements and germline stress. Elife. 2017; doi: 10.7554/eLife.21666
26. Ni JZ, Chen E, Gu SG. Complex coding of endogenous siRNA, transcriptional silencing and H3K9 methylation on native targets of germline nuclear RNAi in C. elegans. BMC Genomics. 2014; doi: 10.1186/1471-2164-15-1157
27. Shirayama M, et al. PiRNAs initiate an epigenetic memory of nonself RNA in the C. elegans germline. Cell. 2012; doi: 10.1016/j.cell.2012.06.015
28. de Albuquerque BFM, Placentino M, Ketting RF. Maternal piRNAs Are Essential for Germline Development following De Novo Establishment of Endo-siRNAs in Caenorhabditis elegans. Dev Cell. 2015; doi: 10.1016/j.devcel.2015.07.010
29. Phillips CM, Brown KC, Montgomery BE, Ruvkun G, Montgomery TA. PiRNAs and piRNA-Dependent siRNAs Protect Conserved and Essential C. elegans Genes from Misrouting into the RNAi Pathway. Dev Cell. 2015; doi: 10.1016/j.devcel.2015.07.009
30. Weick EM, et al. PRDE-1 is a nuclear factor essential for the biogenesis of Ruby motif-dependent piRNAs in C. elegans. Genes Dev. 2014; doi: 10.1101/gad.238105.114
31. Pettitt J, Crombie C, Schümperli D, Müller B. The Caenorhabditis elegans histone hairpin-binding protein is required for core histone gene expression and is essential for embryonic and postembryonic cell division. J Cell Sci. 2002
32. Kodama Y, Rothman JH, Sugimoto A, Yamamoto M. The stem-loop binding protein CDL-1 is required for chromosome condensation, progression of cell death and morphogenesis in Caenorhabditis elegans. Development. 2002
33. Gu W, et al. Distinct Argonaute-Mediated 22G-RNA Pathways Direct Genome Surveillance in the C. elegans Germline. Mol Cell. 2009; doi: 10.1016/j.molcel.2009.09.020
34. Spike CA, Bader J, Reinke V, Strome S. DEPS-1 promotes P-granule assembly and RNA interference in C. elegans germ cells. Development. 2008; doi: 10.1242/dev.015552
35. Shirayama M, Stanney W, Gu W, Seth M, Mello CC. The Vasa homolog RDE-12 engages target mRNA and multiple argonaute proteins to promote RNAi in C. elegans. Curr Biol. 2014; doi: 10.1016/j.cub.2014.03.008
36. Wedeles CJ, Wu MZ, Claycomb JM. Protection of germline gene expression by the C. elegans argonaute CSR-1. Dev Cell. 2013; doi: 10.1016/j.devcel.2013.11.016
37. Seth M, et al. The C. elegans CSR-1 argonaute pathway counteracts epigenetic silencing to promote germline gene expression. Dev Cell. 2013; doi: 10.1016/j.devcel.2013.11.014
38. Avgousti DC, Palani S, Sherman Y, Grishok A. CSR-1 RNAi pathway positively regulates histone expression in C. elegans. EMBO J. 2012; doi: 10.1038/emboj.2012.216

39. Keall R, Whitelaw S, Pettitt J, Müller B. Histone gene expression and histone mRNA 3′ end structure in Caenorhabditis elegans. BMC Mol Biol. 2007; doi: 10.1186/1471-2199-8-51
40. Zhang C, et al. mut-16 and other mutator class genes modulate 22G and 26G siRNA pathways in Caenorhabditis elegans. Proc Natl Acad Sci. 2011; doi: 10.1073/pnas.1018695108
41. Heestand B, Simon M, Frenk S, Titov D, Ahmed S. Transgenerational Sterility of Piwi Mutants Represents a Dynamic Form of Adult Reproductive Diapause. Cell Rep. 2018; doi: 10.1016/j.celrep.2018.03.015
42. Gerson-Gurwitz A, et al. A Small RNA-Catalytic Argonaute Pathway Tunes Germline Transcript Levels to Ensure Embryonic Divisions. Cell. 2016; doi: 10.1016/j.cell.2016.02.040
43. Seth M, et al. The Coding Regions of Germline mRNAs Confer Sensitivity to Argonaute Regulation in C. elegans. Cell Rep. 2018; doi: 10.1016/j.celrep.2018.02.009
44. Tang W, et al. A Sex Chromosome piRNA Promotes Robust Dosage Compensation and Sex Determination in C. elegans. Dev Cell. 2018; doi: 10.1016/j.devcel.2018.01.025
45. Barberán-Soler S, et al. Co-option of the piRNA pathway for germline-specific alternative splicing of C. elegans TOR. Cell Rep. 2014; doi: 10.1016/j.celrep.2014.08.016
46. Sarkies P, et al. Ancient and Novel Small RNA Pathways Compensate for the Loss of piRNAs in Multiple Independent Nematode Lineages. PLoS Biol. 2015; doi: 10.1371/journal.pbio.1002061
47. Tu S, et al. Comparative functional characterization of the CSR-1 22G-RNA pathway in Caenorhabditis nematodes. Nucleic Acids Res. 2015; doi: 10.1093/nar/gku1308
48. Wyler-Duda P, Bernard V, Stadler M, Suter D, Schümperli D. Histone H4 mRNA from the nematode Ascaris lumbricoides is cis-spliced and polyadenylated. Biochim Biophys Acta - Gene Struct Expr. 1997; doi: 10.1016/S0167-4781(96)00235-7
49. Brenner S. The Genetics of Caenorhabditis elegans. Genet. 1974; doi: 10.10.1111/j.1749-6632.1999.tb07894.x
50. Paix A, Folkmann A, Rasoloson D, Seydoux G. High efficiency, homology-directed genome editing in Caenorhabditis elegans using CRISPR-Cas9ribonucleoprotein complexes. Genetics. 2015; doi: 10.1534/genetics.115.179382
51. Arribere JA, et al. Efficient marker-free recovery of custom genetic modifications with CRISPR/Cas9 in caenorhabditis elegans. Genetics. 2014; doi: 10.1534/genetics.114.169730
52. Aoki, K; Moriguchi, H; Okawa, K; Tabara, H. Biochemical genetic analyses of RdRP and Slicer activities related to RNAi in C. elegans. International Worm Meeting; 2007.
53. Edgley, ML, Baillie, DL, Riddle, DL, Rose, AM. Genetic balancersWormBook. C. elegans Res Community. , editor. Wormb; 2006.
54. Kamath RS, Ahringer J. Genome-wide RNAi screening in Caenorhabditis elegans. Methods. 2003; doi: 10.1016/S1046-2023(03)00050-1
55. Jayaprakash AD, Jabado O, Brown BD, Sachidanandam R. Identification and remediation of biases in the activity of RNA ligases in small-RNA deep sequencing. Nucleic Acids Res. 2011; doi: 10.1093/nar/gkr693
56. Cecere G, Hoersch S, O'Keeffe S, Sachidanandam R, Grishok A. Global effects of the CSR-1 RNA interference pathway on the transcriptional landscape. Nat Struct Mol Biol. 2014; 21:358–65. [PubMed: 24681887]
57. Poullet P, Carpentier S, Barillot E. myProMS, a web server for management and validation of mass spectrometry-based proteomic data. Proteomics. 2007; doi: 10.1002/pmic.200600784
58. Valot B, Langella O, Nano E, Zivy M. MassChroQ: A versatile tool for mass spectrometry quantification. Proteomics. 2011; doi: 10.1002/pmic.201100120
59. Cline MS, et al. Cytoscape. Nat Protoc. 2007; doi: 10.1038/nprot.2007.324
60. Vizcaíno JA, et al. 2016 update of the PRIDE database and its related tools. Nucleic Acids Res. 2016; doi: 10.1093/nar/gkv1145
61. Claycomb JM, et al. The Argonaute CSR-1 and Its 22G-RNA Cofactors Are Required for Holocentric Chromosome Segregation. Cell. 2009; doi: 10.1016/j.cell.2009.09.014
62. Kawasaki I, et al. The PGL family proteins associate with germ granules and function redundantly in Caenorhabditis elegans germline development. Genetics. 2004; doi: 10.1534/genetics.103.023093

63. Kim D, Langmead B, Salzberg SL. HISAT: A fast spliced aligner with low memory requirements. Nat Methods. 2015; doi: 10.1038/nmeth.3317
64. Liao Y, Smyth GK, Shi W. FeatureCounts: An efficient general purpose program for assigning sequence reads to genomic features. Bioinformatics. 2014; doi: 10.1093/bioinformatics/btt656
65. Love MI, Huber W, Anders S. Moderated estimation of fold change and dispersion for RNA-seq data with DESeq2. Genome Biol. 2014; doi: 10.1186/s13059-014-0550-8
66. Martin M. Cutadapt removes adapter sequences from high-throughput sequencing reads. EMBnet journal. 2011; doi: 10.14806/ej.17.1.200
67. Langmead B, Salzberg SL. Fast gapped-read alignment with Bowtie 2. Nat Methods. 2012; doi: 10.1038/nmeth.1923
68. Quinlan AR. BEDTools: The Swiss-Army tool for genome feature analysis. Curr Protoc Bioinforma. 2014; doi: 10.1002/0471250953.bi1112s47
69. Neph S, et al. BEDOPS: High-performance genomic feature operations. Bioinformatics. 2012; doi: 10.1093/bioinformatics/bts277
70. Ramírez F, et al. deepTools2: a next generation web server for deep-sequencing data analysis. Nucleic Acids Res. 2016; doi: 10.1093/nar/gkw257

Europe PMC Funders Author Manuscripts

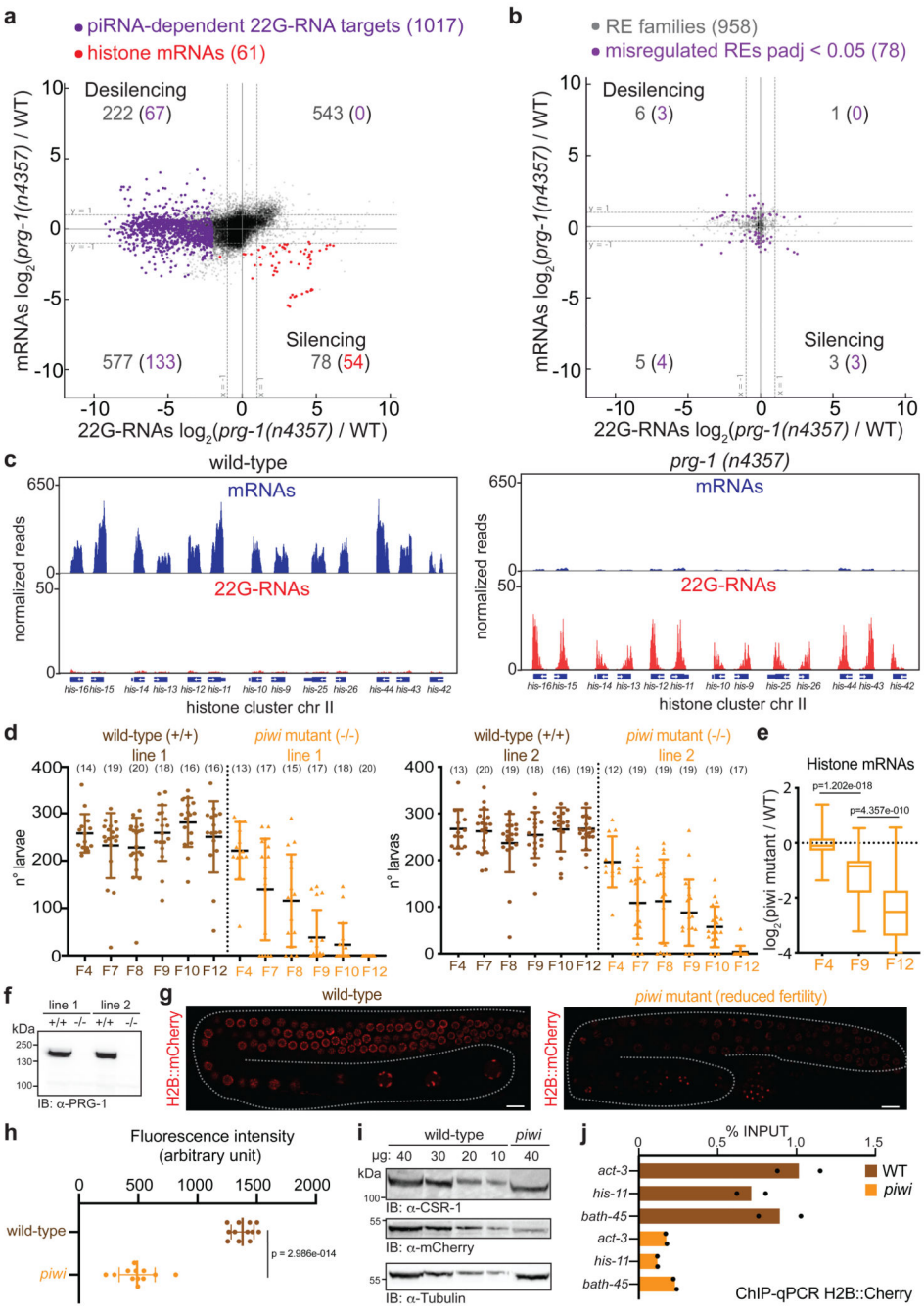

Fig. 1. Histone mRNAs silencing correlates with progressive sterility in *piwi* mutant

a, Comparison between mRNA (y axis) and 22G-RNA (x axis) $\log_2$ fold changes in *prg-1 (n4357)* mutant vs. wild-type worms for protein-coding genes. The dashed lines indicate two-fold changes, and the numbers in parenthesis indicate the portion of misregulated piRNA-dependent 22G-RNA targets (purple) or histone genes (red) (two-fold changes, padj < 0.05, Wald test). The average from two biologically independent replicates is shown. **b**, Similar comparison as in **a** for misregulated RE families (padj < 0.05, Wald test). The average from two biologically independent replicates is shown. **c**, Genomic view of one

Europe PMC Funders Author Manuscripts

histone gene cluster showing mRNAs (blue) and 22G-RNAs (red) in wild-type (left panel) and *prg-1(n4357)* mutant (right panel). **d**, Brood size of the two CRISPR-Cas9 *piwi* mutant (-/-) and wild-type (+/+) lines. Data points correspond to the number of alive larvae from individual worms. The black lines indicate the mean, the error bars the standard deviation. The sample size n (animals) is indicated in parenthesis. **e**, Box plots showing histone mRNAs $\log_2$ fold change in CRISPR-Cas9 *piwi* mutant compared to wild-type across generations. The median (line), first and third quartiles (box) and highest/lowest value (whiskers) are shown. Two-tailed p value was calculated with the Mann-Whitney-Wilcoxon tests, n (number of genes) = 61. **f**, Immunoblot showing PIWI protein in the wild-type and *piwi* mutant lines. The experiment was repeated twice. **g**, **h**, Representative images and quantification of germline-expressed H2B::mCherry in wild-type and *piwi* mutant worms. White bars indicate 10 μM size. Mean intensity from 15 pachytene nuclei in each worm, standard deviation, and two-tailed p value (Unpaired t test) is shown. n = 12 animals. **i**, Immunoblot showing H2B::mCherry in wild-type and *piwi* mutant worms. Ubiquitous (tubulin) and germline (CSR-1) proteins are shown as control. The experiment was repeated twice. **j**, H2B::mCherry ChIP-qPCR in wild-type and *piwi* mutant. The amount of immunoprecipitated DNA is shown as percentage of input. The bars indicate the mean and the black dots individual data from two biologically independent experiments. Source data and unprocessed blots are available in Source Data Fig. 1.

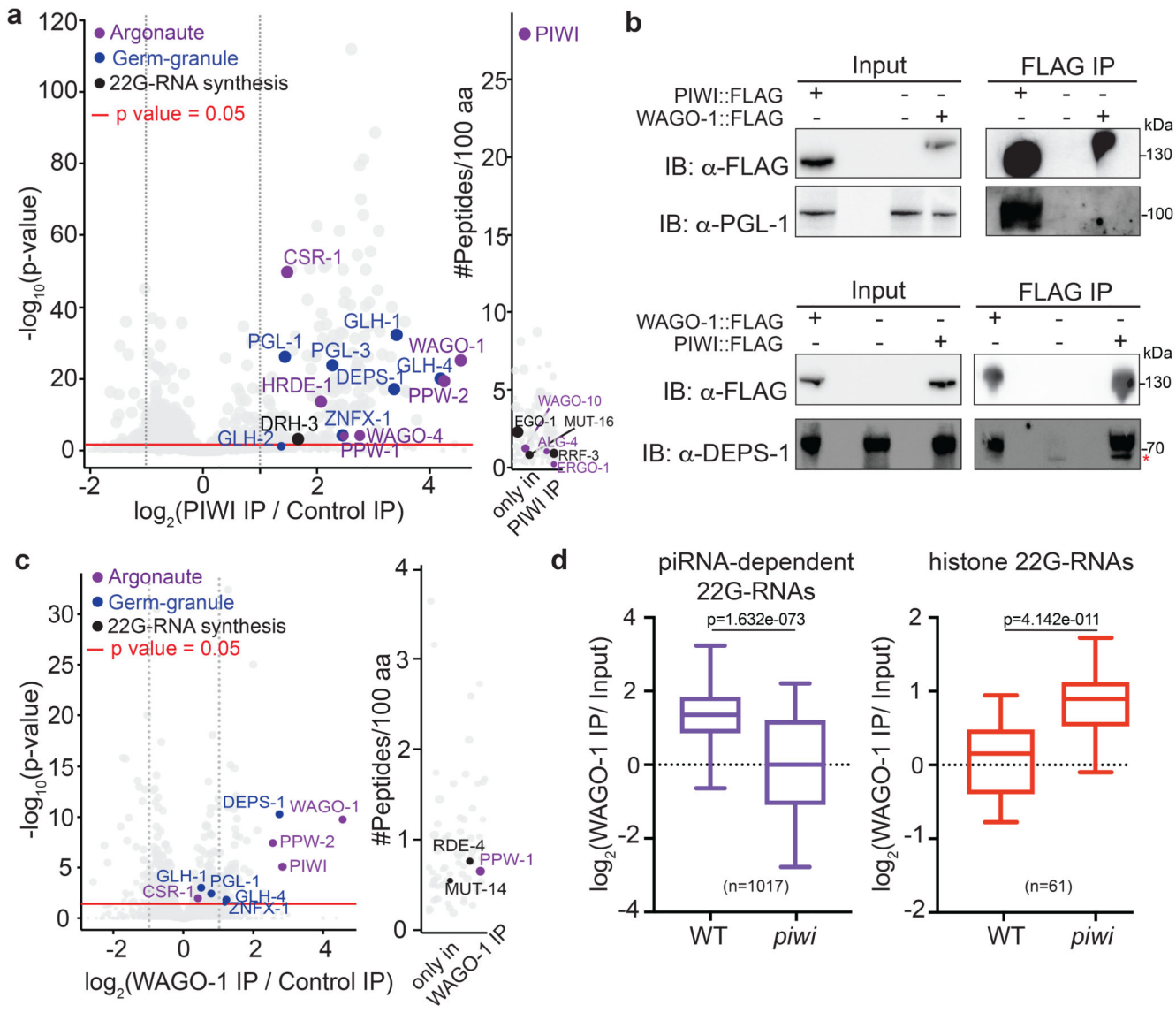

Fig. 2. Loading of histone 22G-RNAs into WAGO-1 upon disruption of the piRNA-induced silencing complex

a, Volcano plot showing enrichment values and corresponding significance levels for proteins co-purifying with PIWI (see also Supplementary Table 1a). Argonaute proteins, germ granule components and 22G-RNA biogenesis factors are labelled with different colours. The size of the dots is proportional to the number of peptides used for the quantification. The linear model was used to compute protein quantification ratio and the red horizontal line indicates the two-tailed p value = 0.05. n = 4 biologically independent experiments. **b**, Co-IP experiments showing DEPS-1 interactions with PIWI and WAGO-1 and PGL-1 interaction with PIWI and not with WAGO-1. Presence (+) or absence (-) of the tagged proteins are indicated. Immunoprecipitation was performed using α-FLAG antibody, and the blots were probed with α-PGL-1, α-DEPS-1 or α-FLAG antibodies. * the lower band signal corresponds to a non-specific protein. The experiment was repeated twice. **c**, Volcano plots showing $\log_2$ fold change and corresponding significance levels of proteins

co-purifying with WAGO-1 in wild-type worm lysate as in **a** (see also Supplementary Table 1b). Argonaute proteins, germ granule components and 22G-RNA biogenesis factors are labelled with different colours. The size of the dots is proportional to the number of peptides used for the quantification. The linear model was used to compute protein quantification ratio and the red horizontal line indicates the two-tailed p value = 0.05. n = 4 biologically independent experiments. **d**, Box plots showing the $\log_2$ fold change of the ratio between piRNA-dependent 22G-RNA and histone 22G-RNA normalized reads from WAGO-1 immunoprecipitation (IP) and total RNA (Input) in wild-type and *piwi* mutant background. The median (line), first and third quartiles (box), and whiskers (5th and 95th percentile) are shown. Two-tailed p value was calculated with the Mann-Whitney-Wilcoxon tests using the sample sizes (number of genes): n = 1017 for piRNA-dependent targets and n = 61 for histone genes. Statistics source data and unprocessed blots are available in Source Data Fig. 2.

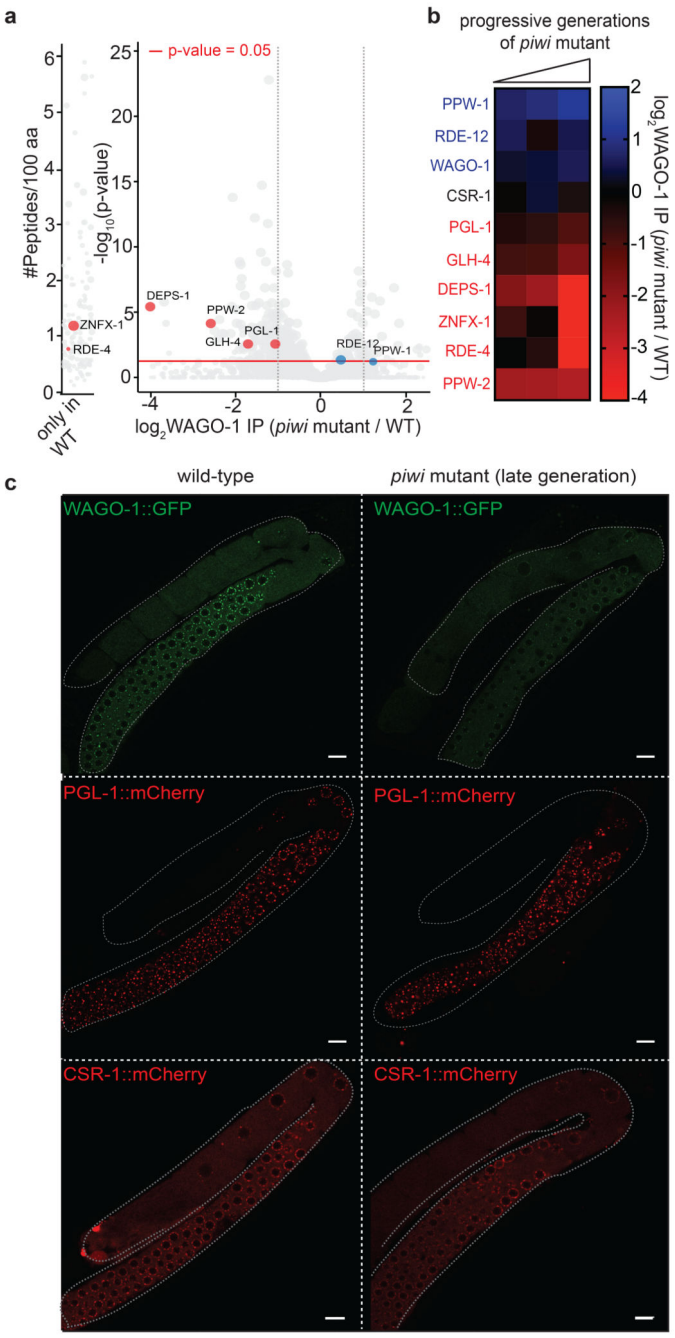

Fig. 3. WAGO-1 loses interactions with germ granule components across generation of *piwi* mutant and remain cytoplasmic

a, Volcano plots showing $\log_2$ fold change and corresponding significance levels of proteins co-purifying with WAGO-1 in *piwi* mutant compared to wild-type. Significant decreased or increased interactions with WAGO-1-interacting germ granule components, Argonaute proteins or RNAi factor are shown in red and blue respectively. The size of the dots is proportional to the number of peptides used for the quantification. The linear model was used to compute protein quantification ratio and the red horizontal line indicates the two-

Europe PMC Funders Author Manuscripts

tailed p value = 0.05. n = 4 biologically independent experiments. **b**, Heatmap showing $\log_2$ fold change of proteins co-purifying with WAGO-1 in *piwi* mutant at different generations compared to wild-type. Decreased or increased interactions with WAGO-1-interacting germ granule components, Argonaute proteins or RNAi factor are shown in red and blue respectively. n = 4 biologically independent experiments. **c**, Live confocal images of WAGO-1::GFP, PGL-1::mCherry, and CSR-1::mCherry showing loss of WAGO-1 germ granule localization in affected *piwi* mutant germlines compared to wild-type. The white bars indicate 10μM size. The experiment was repeated independently three times with similar results. Source data are available in Source Data Fig. 3.

Europe PMC Funders Author Manuscripts

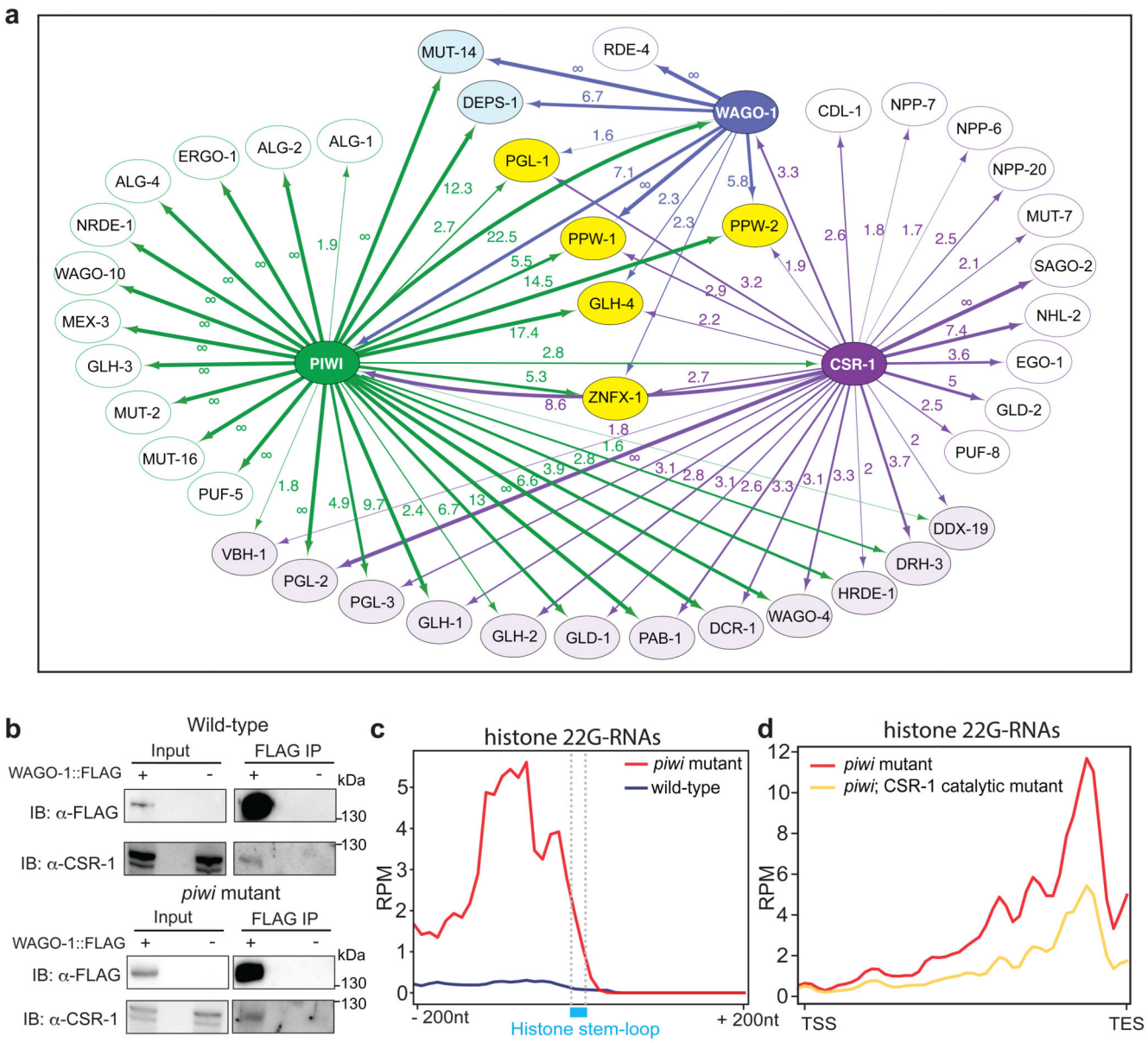

Fig. 4. The CSR-1 pathway triggers the biogenesis of histone 22G-RNAs in *piwi* mutant

a, Network interactome map showing the overlap between CSR-1, PIWI, and WAGO-1 interacting proteins by mass spec. Only a selection of interacting proteins is shown, corresponding to known germ granule components, RNAi factors and Argonaute proteins. Proteins interacting with CSR-1, PIWI and CSR-1 are shown in yellow. Proteins interacting only with PIWI and WAGO are shown in blue. Protein interacting only with CSR-1 and PIWI are shown in light violet. Numbers correspond to enrichment values in IPs and ∞ represents proteins with their peptides detected exclusively in the IP and not in the control. **b**, Co-IP experiments in wild-type (top) and *piwi* mutant (bottom) showing WAGO-1 interactions with CSR-1. Presence (+) or absence (-) of the tagged proteins are indicated. Immunoprecipitation was performed using α-FLAG antibody, and the blots were probed with α-CSR-1 or α-FLAG antibodies. The amount of protein extract for

immunoprecipitation was normalized on the total level of CSR-1 protein because mutant animals have less germline tissue (see also Extended Data Fig. 4e). The experiment was repeated independently two times with similar results. **c**, Metaprofile analysis showing the distribution of normalized 22G-RNA reads (RPM) 200nt upstream and 200nt downstream of the stem-loop sequence of histone mRNAs. The experiment was repeated independently two times with similar results. **d**, Metaprofile analysis showing the distribution of normalized 22G-RNA reads (RPM) across histone genes in *piwi* mutant background with (yellow line) or without (red line) mutation in the catalytic domain of CSR-1. TSS indicates the transcriptional start site, TES indicates the transcriptional end site. The experiment was repeated independently two times with similar results. Statistical source data and unprocessed blots are available in Source Data Fig. 4.

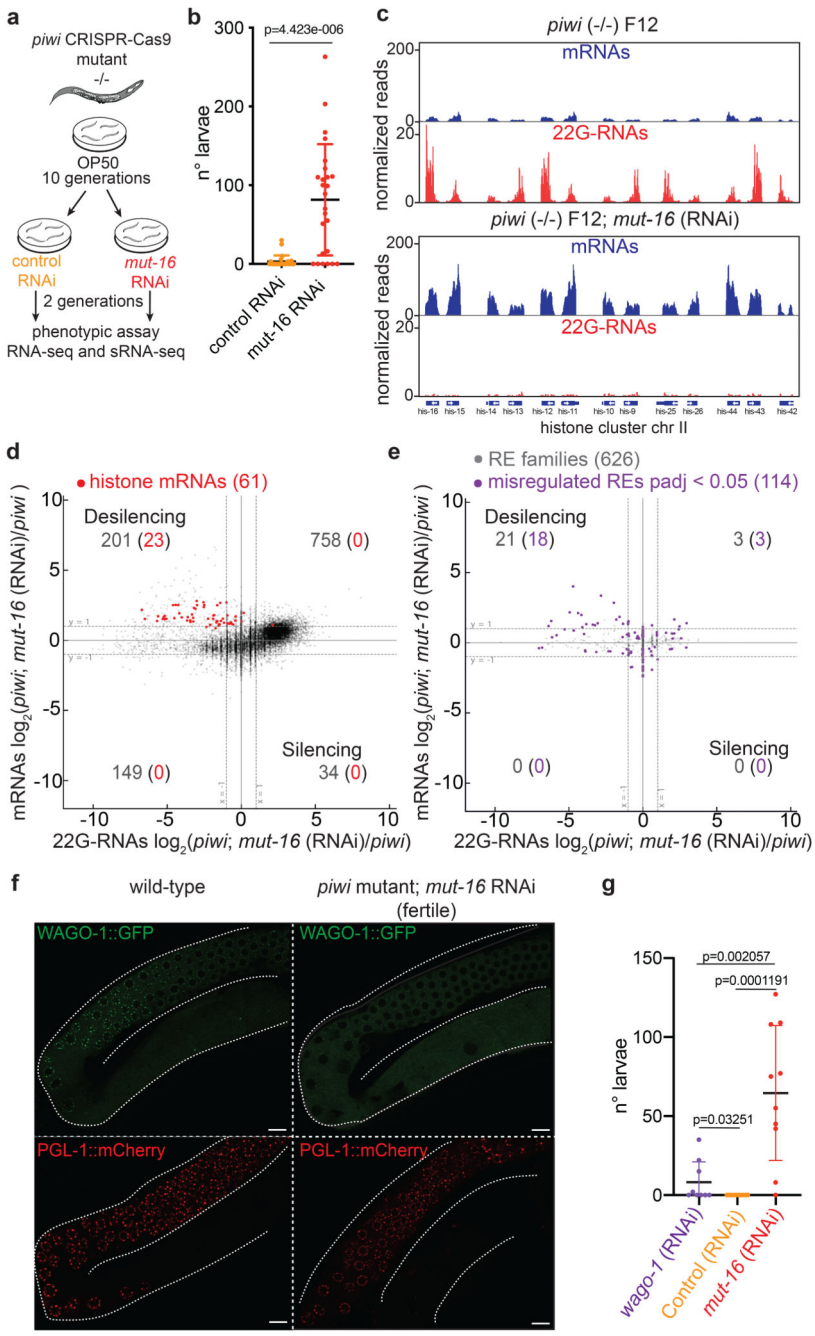

Fig. 5. Removal of histone 22G-RNAs rescues *piwi* mutant transgenerational sterility

a, Schematic of the RNAi experiment using CRISPR-Cas9 *piwi* mutant worms grown for 10 generations on plates seeded with *E. coli* OP50 and then shifted for two generations on plates seeded with *mut-16* or control RNAi food. **b**, Results from brood size assay of the experiment described in **a**. Each dot corresponds to the number of alive larvae from individual worms. The black lines indicate the average brood size and the error bars the standard deviation. Two-tailed p value calculated using Mann-Whitney-Wilcoxon tests is shown. Sample size n = 25 animals. **c**, Genomic view similar to Fig. 1c of one histone

Europe PMC Funders Author Manuscripts

cluster in *piwi* mutant F12 (upper panel) or treated with *mut-16* RNAi (lower panel). **d**, Comparison between mRNA (y axis) and 22G-RNA (x axis) $\log_2$ fold changes in *piwi* mutant F12 treated with *mut-16* RNAi vs. *piwi* mutant F12. The dashed lines indicate the two-fold changes, and the number in parenthesis indicates the portion of misregulated genes (two-fold changes, padj < 0.05, Wald test) belonging to the histone genes (red). The average from two biologically independent replicates is shown. **e**, Same comparison as in **d**, except that families of REs were analysed. The purple dots indicate significantly misregulated RE families by RNA-seq (padj < 0.05, Wald test). The average from two biologically independent replicates is shown. **f**, Live confocal images of WAGO-1::GFP and PGL-1::mCherry showing lack of WAGO-1 germ granule localization in fertile *piwi* mutant upon *mut-16* RNAi treatment compared to wild-type. The white bars indicate 10 μM size. The experiment was repeated independently three times. **g**, Results from brood size assay similar to the experiment described in **a**, except that sterile *piwi* mutant worms were used for the assay. Each dot corresponds to the total number of alive larvae from an individual worm. The black lines indicate the average brood size and the error bars the standard deviation. Two-tailed p value calculated using Mann-Whitney-Wilcoxon tests is shown. Sample size n = 10 animals. Source data are available in Source Data Fig. 5.

Europe PMC Funders Author Manuscripts

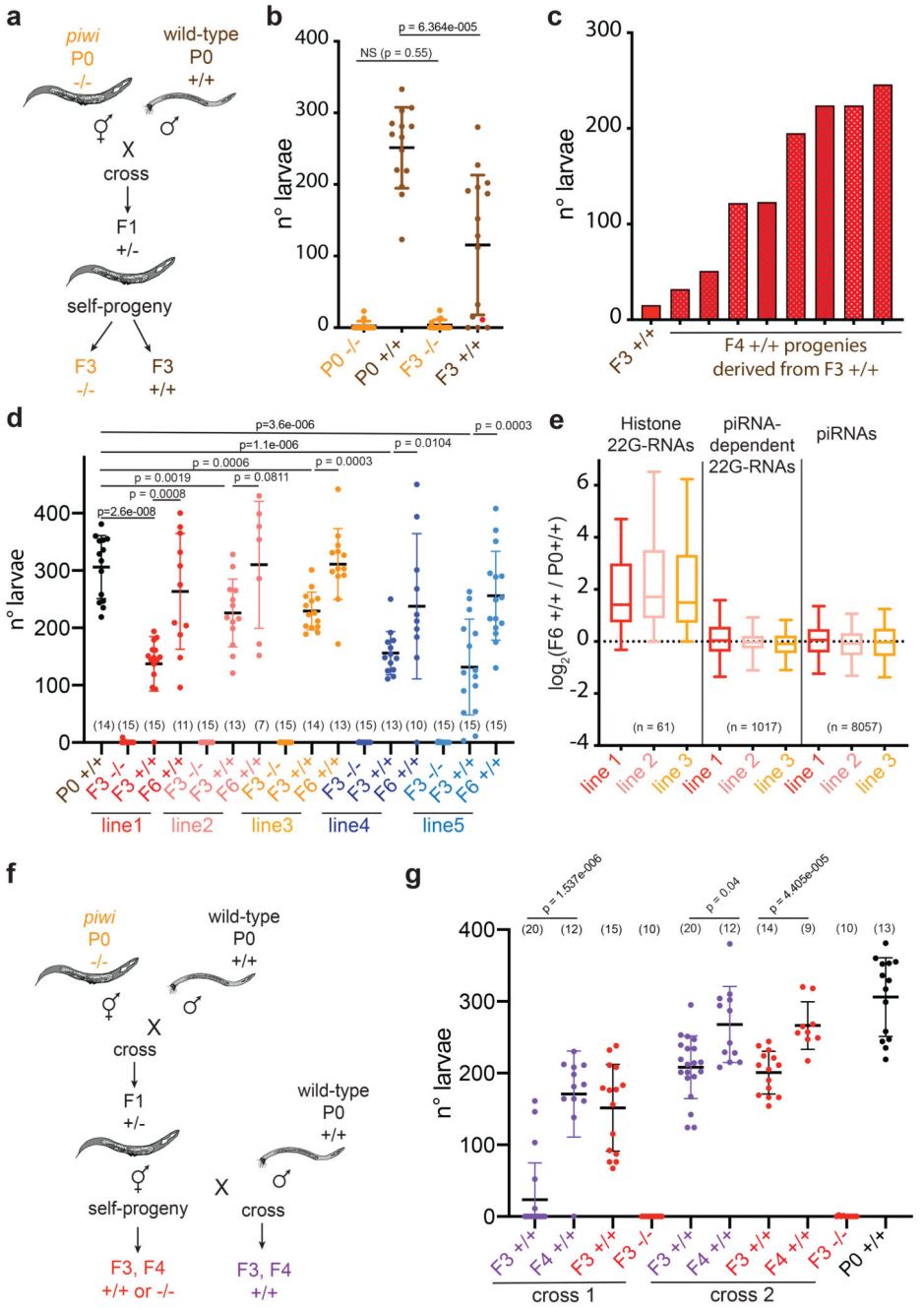

Fig. 6. Histone 22G-RNAs facilitate the epigenetic inheritance of a *piwi*-like phenotype in wild-type worms

a, Schematic of cross between wild-type males (+/+) and almost sterile hermaphrodite *piwi* (*prg-1(4357)* or CRISPR-Cas9) mutants (-/-). **b**, Brood size assay of the cross experiment described in **a**. Each dot corresponds to the number of alive larvae from individual worms. The black lines indicate the mean and the error bars the standard deviation. Two-tailed p value calculated using the Mann-Whitney-Wilcoxon tests is shown. Sample size n = 15 animals. **c**, Brood size assay as in **b**, showing the brood of all the individual F4 +/+ animals

Europe PMC Funders Author Manuscripts

(red bars) derived from the same F3 +/+ parental worm (also shown in **b**, as red dot). **d**, Brood size assay as in **b** of the cross experiment described in **a**, using five selected F2 wild-type crossed lines (+/+). The black lines indicate the mean, the error bars the standard deviation, and the sample size n (animals) is indicated in parenthesis. Two-tailed p value calculated using the Mann-Whitney-Wilcoxon tests is shown. **e**, Box plots of small RNA $\log_2$ fold change in F6 +/+ crossed line 1 (red), line 2 (pink) and line 3 (yellow) compared with the parental P0 +/+. 22G-RNAs antisense to histone mRNAs, piRNA-dependent mRNA targets, and piRNAs are shown. The median (line), first and third quartiles (box), and whiskers (5th and 95th percentile) are shown. The number of genes in each category is indicated in parenthesis. **f**, Schematic of cross between wild-type males (+/+) and hermaphrodite heterozygote *piwi* mutant (+/-) (purple) or self-progeny (red). After the cross wild-type (+/+) lines or self-crossed wild-type (+/+) and *piwi* mutant (-/-) lines were selected. Wild-type (+/+) lines were propagated for 2 generations (F3-F4). **g**, Brood size assay as in **b** of the cross experiment described in **f**. The black lines indicate the mean and the error bars the standard deviation. Two-tailed p value calculated using the Mann-Whitney-Wilcoxon tests is shown. Sample size n (animals) is indicated in parenthesis. Source data are available in Source Data Fig. 6.